Check for updates

The FEBS Journal

FEBS PRESS science publishing by scientists

The sorting nexin Snx21 promotes flotillin-mediated endocytosis

Tamás Maruzs[1], Enikő Lakatos[1,2], Dalma Feil-Börcsök[1], Gábor Juhász[1], Regina Mező[1], Asha Kiran Maddali[1], András Blastyák[1], Aladár Pettkó-Szandtner[3], Hajnalka Laczkó-Dobos[1] and Gábor Juhász[1,4]

1 Institute of Genetics, HUN-REN Biological Research Centre, Szeged, Hungary
2 Doctoral School of Biology, University of Szeged, Hungary
3 Laboratory of Proteomics, Complex Molecular and Cell Biology Service Centre, HUN-REN Biological Research Centre, Szeged, Hungary
4 Department of Anatomy, Cell and Developmental Biology, Eötvös Loránd University, Budapest, Hungary

Keywords
Drosophila; endocytosis; flotillin; Snx21; vesicle trafficking

Correspondence
T. Maruzs and G. Juhász, Institute of Genetics, HUN-REN Biological Research Centre, Szeged, H-6726 Hungary
E-mail: maruzs.tamas@brc.hu and juhasz.gabor@brc.hu

Tamás Maruzs and Enikő Lakatos contributed equally to this work.

(Received 4 November 2025, revised 26 March 2026, accepted 4 June 2026)

doi:10.1111/febs.70618

Upregulation of flotillins, the defining proteins of an incompletely characterized clathrin-independent form of endocytosis, is reported in a variety of human pathologies such as cancer, neurodegeneration, and infection. Several sorting nexin (Snx) proteins have established roles in the endosomal network, but the function of many members of this phospholipid-binding protein family such as Snx21 is still poorly investigated. Here, we show that Snx21 binds to the phospholipid PI(3)P enriched in endosomal membranes, and it localizes to the endosomal system in various Drosophila tissues. We find that Snx21 also binds to and colocalizes with flotillins in Drosophila. We propose that overexpression of Snx21 facilitates endocytic trafficking toward late endosomes/lysosomes leading to a large increase in the size of late endosomes, which requires Flotillin2. In parallel, Snx21 is required for multiple alterations caused by Flotillin2 overexpression: both the intracellular accumulation of Wingless/Wnt morphogen and ectopic wing vein formation that are induced by Flotillin2 overexpression in the developing wing depend on Snx21. Taken together, we identify Snx21 as a previously undescribed physical and functional interacting partner of flotillins, and our data point to the role of Snx21 as a potential positive regulator of flotillin-mediated endocytic trafficking.

Introduction

During endocytosis, eukaryotic cells take up liquid-phase material from their environment. This way, extracellular components including nutrients and various signaling molecules enter the cell as endocytic cargo and are processed within the endosomal system. Continuous flow of material in the endosomal network is a prerequisite of normal cell function and is accompanied by a complex series of fusion and fission events summarized under the term of endosomal maturation [1]. As the first step of this process, small portions of the extracellular fluid are taken up by invaginations of the plasma membrane and are subsequently pinched off. Although the formed primary endocytic vesicles represent a heterogeneous

Abbreviations
CRAC, cholesterol-recognizing amino acid consensus; Flo1/Reggie2, Flotillin1; Flo2/Reggie1, Flotillin2; Hh, Hedgehog; LTR, Lysotracker Red; PBTx, Triton X-100 in PBS; PI, phosphoinositide; [PI(3,4,5)P_3], phosphatidylinositol (3,4,5)-trisphosphate; [(PI(3,4)P_2)], phosphatidylinositol (3,4)-bisphosphate; [PI(3,5)P_2], phosphatidylinositol (3,5)-bisphosphate; [PI(3)P], phosphatidylinositol 3-phosphate; PX, Phox-homology; PXB, PX-associated B; Snx, sorting nexin; SPFH, stomatin, prohibitin, flotillin, HflK/C; TCA, trichloroacetic acid; TPR, tetratricopeptide repeat; UFIT, upregulated flotillin trafficking; Wg, wingless.

© 2026 The Author(s). *The FEBS Journal* published by John Wiley & Sons Ltd on behalf of Federation of European Biochemical Societies.
This is an open access article under the terms of the Creative Commons Attribution-NonCommercial-NoDerivs License, which permits use and distribution in any medium, provided the original work is properly cited, the use is non-commercial and no modifications or adaptations are made.

population based on their content and the molecular mechanism of their formation, these follow common routes during endosomal maturation. They fuse with each other to create early endosomes where sorting of the endosomal content starts with the formation of membrane tubules. These dynamic structures separate components to be recycled back to the plasma membrane, while the vesicular part of the endosome retains material destined for degradation. These traffic to late endosomes and ultimately fuse with lysosomes, where degradation of the cargo is executed by lysosomal hydrolases.

Throughout the course of endosomal maturation, the composition of the endosomal membrane undergoes remarkable changes [2]. One aspect of this process is the gradual shift of the phosphoinositide (PI) profile during the consecutive steps of the maturation process. While the early endosomal membrane is enriched in phosphatidylinositol 3-phosphate [PI(3)P], this lipid moiety is then converted to phosphatidylinositol (3,5)-bisphosphate [$PI(3,5)P_2$], the defining PI-type of late endosomes. Phosphorylation of PIs is mediated by kinases that are recruited to endosomal membranes as the effectors of Rab proteins. PI(3)P is generated mainly by the Rab5 effector Vps34, a class III phosphatidylinositol 3-kinase. PI(3)P subsequently recruits PIKfyve, a phosphatidylinositol 3-phosphate 5-kinase that creates $PI(3,5)P_2$. The activity of the players of this molecular cascade leads to the dissociation of Rab5 from and the recruitment of Rab7 to the endosomal membrane. The resulting switch of Rab5 to Rab7 gives a novel identity for the endosomes (early vs. late endosome, respectively) and enables the recruitment of the next group of effector proteins including the mediators of late endosome-lysosome fusion [3]. Thus, endosomal maturation is propelled by a molecular cascade with the cooperation of several proteins and multiprotein complexes. Perturbations of this delicate system (e.g., due to mutations) lead to disturbed cell function and to the pathogenesis of severe diseases such as cancer and neurodegeneration [4].

Although the main steps and features of endosomal maturation follow the above general scheme in most cell types, different forms of endocytosis can be distinguished based on the molecular players involved in the formation of primary endocytic vesicles [5]. Besides the well-known clathrin-mediated endocytosis, other mechanisms exist in which primary endocytic vesicles are formed without clathrin coats and are generated with the contribution of different structural proteins. One of such special proteins is flotillins that can induce membrane curvature upon their association with cholesterol- and sphingolipid-enriched membrane microdomains (lipid rafts) [6]. In the flotillin-mediated endocytosis pathway, flotillin heterooligomers assemble at the cytosolic face of membranes and induce the formation of invaginations that subsequently bud to the cytoplasm as vesicles. Flotillin oligomers consist of the highly conserved Flotillin 1 (Flo1/Reggie2) and Flotillin2 (Flo2/Reggie1) membrane proteins that are ubiquitously expressed in mammals with enrichment in the nervous system, muscle/adipose tissue and erythrocytes [7,8]. Flo1 and Flo2 share approx. 48% of sequence identity and are structurally very similar to each other [6]. Both proteins contain an N-terminal SPFH (stomatin, prohibitin, flotillin, HflK/C) domain that is mainly responsible for membrane association, while the C-terminal flotillin-domain enables oligomerization. Membrane association is primarily mediated by palmitoylated and myristoylated residues and supported by hydrophobic stretches and cholesterol-recognizing amino acid consensus (CRAC) motifs, while oligomerization involves the coiled coil regions of the proteins. Recent studies [9,10] provided a model of flotillin oligomer assembly, in which a complex of 22 copies of flotillin dimers co-assemble and form a truncated cone-shaped cage on the cytosolic leaflet of the phospholipid bilayer. This model provides the basis for a new mechanism on how these proteins may mediate remodeling of intracellular membranes.

Depending on the cell type, the intracellular distribution of flotillins is diverse and highly dynamic. Besides the plasma membrane where flotillins are enriched at cellular contact sites, they can also be found in many other organelles such as the Golgi apparatus, endoplasmic reticulum, endosomes, lysosomes, and exosomes [11–15]. Based on their function in various aspects of membrane trafficking, flotillin proteins are involved in cell–cell adhesion, cellular signaling, differentiation, and axon regeneration. Flotillins also interact with actin-binding proteins to influence actin dynamics and to regulate adhesion, cell shape, and motility [16–20]. Despite their involvement in many key cellular processes, loss of flotillin function does not always cause severe phenotypes: For example, flotillin knockout mice are viable and fertile [21,22]. It is thought that the absence of flotillin function can be compensated by other SPFH-domain containing proteins, which thus hinders the functional analysis of flotillins [12]. On the other hand, in many cases, upregulation of flotillins is linked to cellular pathology that led to the proposal of the upregulated flotillin trafficking (UFIT) term [23]. Although flotillin upregulation in cancer, neurodegenerative and infectious diseases is well-established [24,25], the exact molecular mechanism of flotillin action is not precisely

© 2026 The Author(s). *The FEBS Journal* published by John Wiley & Sons Ltd on behalf of Federation of European Biochemical Societies.

17424658, 0, Downloaded from https://febs.onlinelibrary.wiley.com/doi/10.1111/febs.70618 by HUN-REN Biological Research Center, Szeged, Wiley Online Library on [25/11/2026]. See the Terms and Conditions (https://onlinelibrary.wiley.com/terms-and-conditions) on Wiley Online Library for rules of use; OA articles are governed by the applicable Creative Commons License

understood and new interacting partners of flotillins also remain to be characterized.

Among the many molecular players involved in endosomal trafficking, Sorting nexin (Snx) proteins represent an evolutionarily conserved family that is classified in a common group by the presence of their lipid-binding phox-homology (PX) domain [26]. Canonically, the PX-domain preferentially binds PI(3)P, although noncanonical PX-domains are also described with altered phosphoinositide-binding properties [27]. Membrane association of most Snx proteins is mediated at least in part by the PX-domain, although other domains are also present in different members of the family. These structural/functional protein modules enable the involvement of Snx proteins in a myriad of cellular functions and provide the basis of their classification into different subgroups [28]. For example, BAR-domain containing Snx proteins can sense and/or create membrane curvature, making these proteins intensively studied, important factors in membrane trafficking events of the endosomal system [29]. In contrast, members of other Snx subgroups are still poorly characterized.

Members of the PXB Snx subfamily: SNX20 (SLIC-1) and SNX21 (SNX-L) in mammals have only a sole PX-associated B (PXB) domain beside their PX-domain [26]. The structure and membrane binding properties of both proteins were analyzed [30], and an atypical tetratricopeptide repeat (TPR)-fold was found in the PXB-domain. Based on the presence of this protein–protein interaction module, the scaffolding property of SNX20 and SNX21 was proposed, and in line with this, a sole research article was published about SNX21, describing it as an early endosomal scaffolding protein [31]. This study demonstrated the interaction between the N-terminal part of SNX21 and Huntingtin, while its PXB domain interacts with septins, a family of cytoskeletal- and membrane-associated proteins [32]. The potential role of SNX21 in receptor degradation during human liver development was also proposed [33]. Little is known about the function of SNX20: A single experimental study found its function in the endosomal trafficking of PSGL-1, a selectin-binding protein that is involved in adhering blood cells to the endothelial lining [34]. SNPs in the SNX20 locus have been associated with inflammatory bowel disease [35], and upregulation of SNX20 was described in lung adenocarcinoma [36,37] and glioma [38]. Further experimental evidence is lacking about the exact molecular functions of the PXB Snx proteins.

In this study, we describe a novel function of the previously uncharacterized Snx21, the single PXB Snx protein in Drosophila as a potential positive regulator of flotillin-mediated endocytosis. We demonstrate that Snx21 physically interacts with flotillins in the endosomal system of fruit fly tissues and that Snx21 is required for the effect of flotillin overexpression resulting in the intracellular accumulation of the Wingless (Wg) morphogen. We also show that excess Snx21 leads to the expansion of endosomal populations in a Flo2-dependent manner. We thus propose that the cooperation of Snx21 and flotillins is involved in a subset of endosomal trafficking events.

Results

Snx21 binds to PI(3)P, localizes to endosomes, and its overexpression leads to the expansion of late endosomal/lysosomal compartments in Drosophila tissues

To test the lipid binding preference of Drosophila Snx21, we have purified the full-length recombinant protein and used it in flotation assay experiments (Fig. 1) after incubation with liposomes containing various phosphoinositide species: phosphatidylinositol 3-phosphate [PI(3)P], enriched on early endosomes, phosphatidylinositol (3,5)-bisphosphate [PI(3,5)P_2], a marker primarily for late endosomes and lysosomes, and phosphatidylinositol (3,4)-bisphosphate [(PI(3,4)P_2)] and phosphatidylinositol (3,4,5)-trisphosphate [PI(3,4,5)P_3], which are key second messengers at the plasma membrane [39]. Snx21 remained in the lower region (8–12 fractions) when it was subjected to sucrose gradient centrifugation in the absence of liposomes or with neutral lipid-containing liposomes (PC and PE) (Fig. 1A,B). In contrast, when incubated with liposomes containing PI(3)P, the protein floated to the top along with the liposomes (Fractions 1–7) (Fig. 1C). Snx21 did not show obvious binding to liposomes containing PI(3,5)P_2, PI(3,4)P_2, or PI(3,4,5)P_3 [Fig. 1D–F]. These results show that *Drosophila* Snx21 has a strong affinity for PI(3)P *in vitro*, suggesting that it is primarily recruited to early endosomal membranes.

Next, we analyzed the localization of Snx21 in larval fruit fly tissues *in vivo*. For this, we have generated UAS-driven, full-length Snx21 reporters with GFP fused to the N- or C-terminal end of the Snx21 coding region. According to FlyBase, two isoforms are annotated in the case of the *snx21* locus: Snx21-PA and Snx21-PB as 326 and 320 amino acid long polypeptides, respectively. To create our Snx21 reporters, we used the sequence of the longer, PA isoform. After the establishment of transgenic stocks, we first used the

© 2026 The Author(s). *The FEBS Journal* published by John Wiley & Sons Ltd on behalf of Federation of European Biochemical Societies.

17424658, 0, Downloaded from https://febs.onlinelibrary.wiley.com/doi/10.1111/febs.70618 by HUN-REN Biological Research Center, Szeged, Wiley Online Library on [25/11/2026]. See the Terms and Conditions (https://onlinelibrary.wiley.com/terms-and-conditions) on Wiley Online Library for rules of use; OA articles are governed by the applicable Creative Commons License

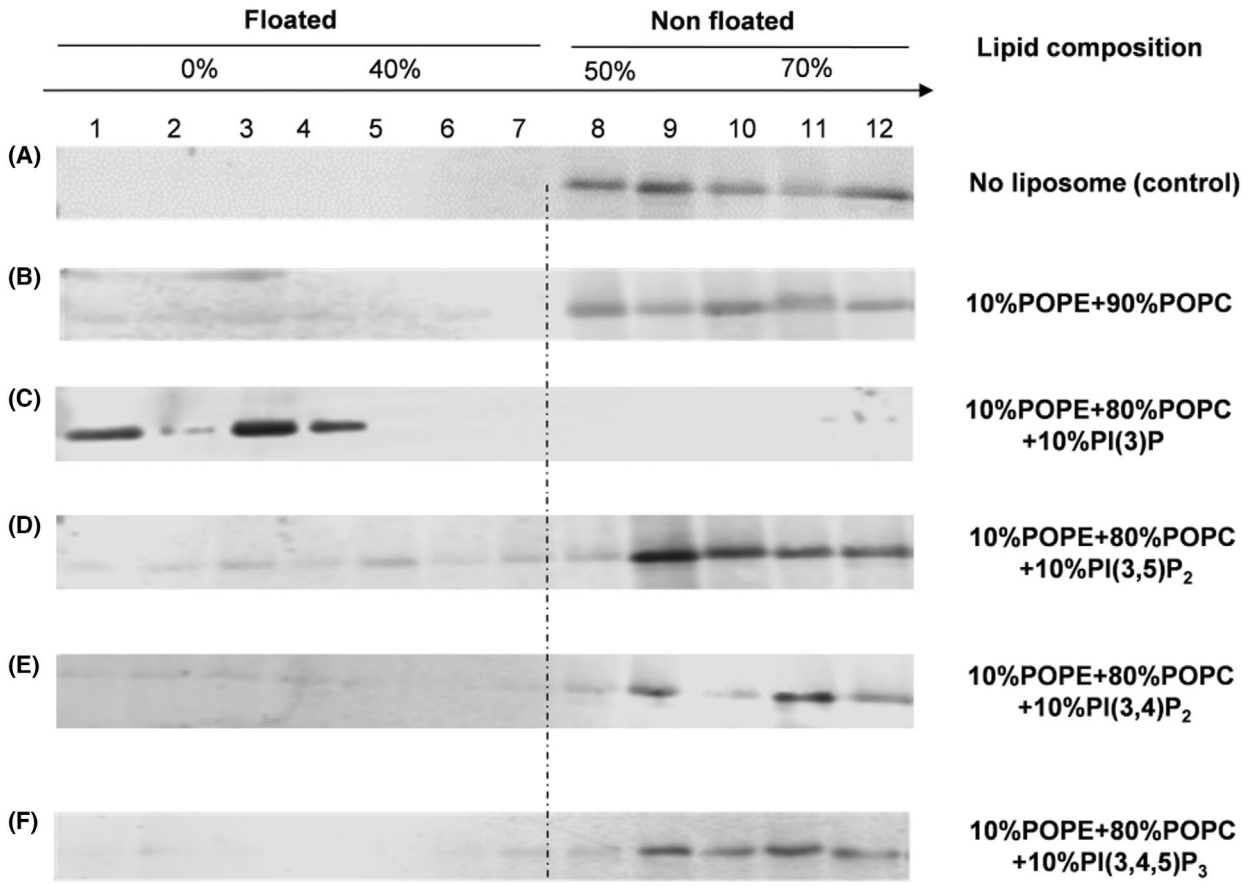


Fig. 1. Snx21 preferentially binds PI(3)P. (A–F) Lipid flotation assay using the indicated liposome compositions. Incubation of recombinant full-length Drosophila GST-Snx21 protein with liposomes was followed by sucrose density gradient ultracentrifugation and anti-GST western blot. Floated fractions are indicated by a dashed line. In the absence of liposomes (A) or with neutral lipid-based (PC and PE) liposomes (B), Snx21 remains in the lower region of the gradient (Fractions 8–12). However, when incubated with liposomes containing PI(3)P, an early endosome marker (C), Snx21 floats to the top along with the liposomes (fractions 1–7). Snx21 does not bind to liposomes containing PI(3,5)P_2 (D), PI(3,4)P_2 (E), or PI(3,4,5)P_3 (F). Representative images of three independent experiments, all with similar results.

ubiquitous tubulin-Gal4 driver for the expression of UAS-GFP-Snx21 or UAS-Snx21-GFP in all tissues. Both reporters showed a predominantly vesicular localization in all investigated larval cell types, and the pattern of the N-terminally tagged protein was indistinguishable from that of the C-terminally tagged version (Fig. S1), which we used in our further experiments. We then dissected salivary glands, fat body lobes and midgut sections from third instar larvae and immunostained them for established markers of endosomal populations (Fig. 2). Overlap of ring-like Snx21-GFP-positive structures and Rab5-positive early endosomes was only evident in the salivary gland (Fig. 2A, yellow arrows), while Rab5-positive dots appeared mostly in the close vicinity of Snx21-GFP-positive rings with rare precise overlap in fat and intestinal cells (Fig. 2C,E, blue arrows). Extensive colocalization of our Snx21-GFP reporter was observed with the late endosomal marker Rab7 in all investigated tissues (Fig. 2H,J,L, yellow arrows). Lamp1-positive lysosomes also often appeared close to the Snx21-GFP-positive vesicles in the fat body and the midgut (Fig. 2Q,S, arrowheads), while significant overlap was only seen in the salivary gland (Fig. 2O). Quantification (Fig. 2G,N,U) also confirms that Pearson's correlation coefficient is the highest in the case of the late endosomal Rab7 marker in all cell types. Importantly, Snx21 had a strong effect on the pattern of the late endosomal population: overexpression of Snx21-GFP led to the significant increase of Rab7-positive structures in all investigated tissues (Fig. 2H", J",L") when compared to control cells (Fig. 2I,K,M).

© 2026 The Author(s). *The FEBS Journal* published by John Wiley & Sons Ltd on behalf of Federation of European Biochemical Societies.

17424658, 0, Downloaded from https://febs.onlinelibrary.wiley.com/doi/10.1111/febs.70618 by HUN-REN Biological Research Center, Szeged, Wiley Online Library on [25/11/2026]. See the Terms and Conditions (https://onlinelibrary.wiley.com/terms-and-conditions) on Wiley Online Library for rules of use; OA articles are governed by the applicable Creative Commons License

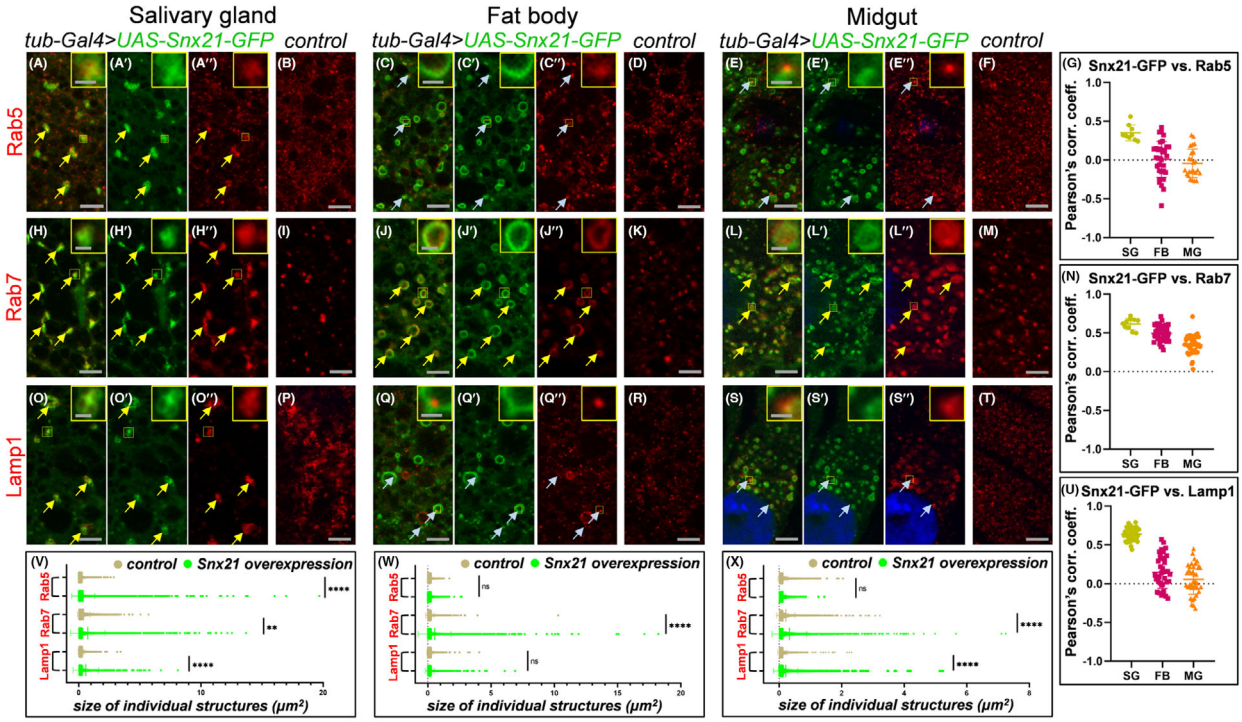


Fig. 2. Snx21 localizes to late endosomes *in vivo* and its overexpression leads to the expansion of late endosomal/lysosomal populations in Drosophila tissues. (4.8.) Snx21-GFP expressing and control salivary glands, fat tissue and midgut sections of third instar larvae immunostained for markers of different endosomal populations. Magnifications of the indicated areas (yellow rectangles) are shown as insets in the upper right corners. Overlap (yellow arrows) of ring-like Snx21-GFP-positive structures and Rab5-positive early endosomes is only evident in the salivary gland (A), while in the fat body and the midgut, Rab5-positive dots frequently appear in the close vicinity (blue arrows) of Snx21-GFP-positive rings with minimal to no overlap (C, E). Snx21-GFP shows extensive colocalization with the late endosomal marker Rab7 in all investigated tissues (H, J, L). Lamp1-positive lysosomes also appear close to the Snx21-GFP-positive vesicles in fat and intestinal tissues (Q, S), while significant overlap is only apparent in the salivary gland (O). (G, N, U) Quantification of Pearson's correlation coefficients (mean ± SD) of Snx21-GFP and endosomal markers in tissues represented in (A, C, E), (H, J, L) and (O, Q, S); SG—salivary gland, FB—fat body tissue, MG—midgut. Overexpression of Snx21-GFP leads to the significant enlargement of Rab7-positive structures in all investigated tissues (h", j", l") when compared to controls (I, K, M). Increased early endosomal size compared to control tissues (B, D, F) is only seen in the salivary glands (A" vs. B), while Lamp1-positive lysosomes are enlarged compared to control tissues (P, R, T) both in Snx21-GFP expressing salivary glands (O" vs. P) and midguts (S" vs. T). (V, W, X) Quantification of individual sizes of Rab5-, Rab7- or Lamp1-positive structures in the investigated tissues represented in (A–F, H–M, O–T). Mann–Whitney *U* test; mean ± SD. * means $P < 0.05$; ** means $P < 0.01$; *** means $P < 0.001$, **** means $P < 0.0001$. Scale bars represent 5 μm and 1 μm (insets).

Quantification (Fig. 2V,W,X) revealed ~1.8-fold, ~3.5-fold, and ~1.5-fold increases in the average size of late endosomes in the salivary gland, fat body, and midgut, respectively. Regarding the other two endosomal compartments, the effect of Snx21 overexpression varied depending on the cell type. Early endosomal size only increased in the salivary glands (Fig. 2A" vs. Fig. 2B), but not in the fat body (Fig. 2C" vs. Fig. 2D) or the midgut (Fig. 2E" vs. Fig. 2F), while Lamp1-positive lysosomes were enlarged in Snx21-GFP expressing salivary glands (Fig. 2O" vs. Fig. 2P) and midguts (Fig. 2S" vs. Fig. 2T), but not in the case of fat tissue (Fig. 2Q" vs. Fig. 2R). These results show that Snx21 functions within the endosomal system of multiple Drosophila tissues, where it primarily localizes to late endosomes, and its overexpression leads to the expansion of endosomal compartments with a major effect on late endosomes.

To analyze whether the loss of Snx21 function perturbs the endosomal system of fruit fly tissues, we used two independent RNAi constructs targeting different regions of the Snx21 mRNA. First, we tested the knockdown efficiency of these constructs using the Snx21-GFP transgene (Fig. 3A). Expression of Snx21-GFP in salivary glands could be readily detected in prepupae of the *prospero-Gal4, UAS-Snx21-GFP* recombinant stock and in prepupae coexpressing a Luciferase knockdown (Luc KD) construct as RNAi

© 2026 The Author(s). *The FEBS Journal* published by John Wiley & Sons Ltd on behalf of Federation of European Biochemical Societies.

17424658, 0, Downloaded from https://febs.onlinelibrary.wiley.com/doi/10.1111/febs.70618 by HUN-REN Biological Research Center, Szeged, Wiley Online Library on [25/11/2026]. See the Terms and Conditions (https://onlinelibrary.wiley.com/terms-and-conditions) on Wiley Online Library for rules of use; OA articles are governed by the applicable Creative Commons License

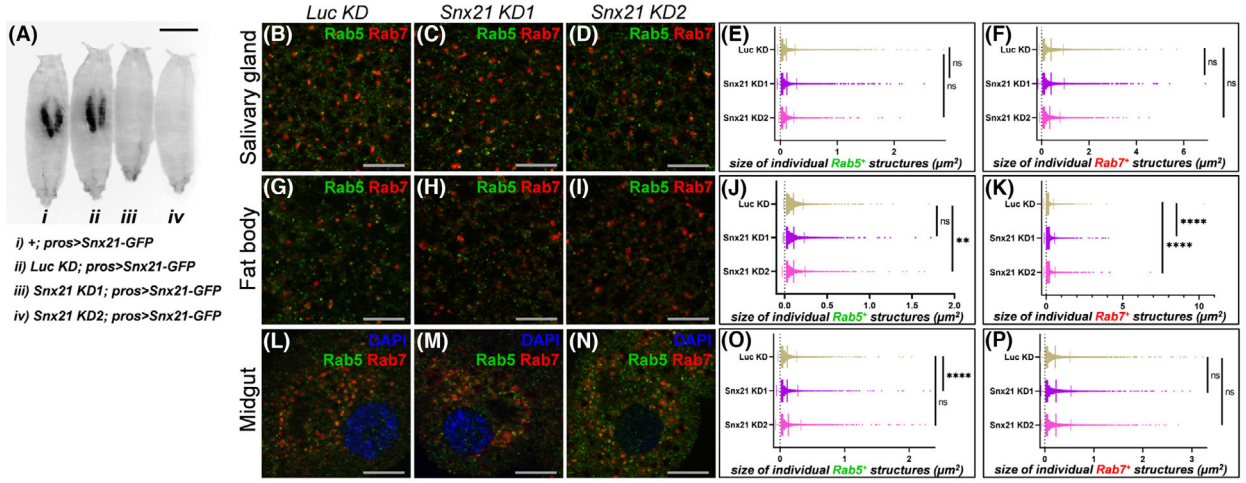


Fig. 3. Snx21 loss does not affect endolysosomal compartments. (A) Expression of Snx21-GFP in the salivary glands of control and Snx21 knockdown prepupae. High amounts of GFP-fusion protein are present in animals expressing UAS-Snx21-GFP driven by prospero-Gal4 (i) and in animals coexpressing Luciferase RNAi as an additional control (ii). Snx21-GFP expression is completely lost in animals coexpressing either one of the Snx21 RNAi constructs: KD1 (iii) or KD2 (iv), indicating efficient elimination of the Snx21 protein. (B–D), (G–I), and (L–N) Organization of the endosomal system in control (B, G, L), Snx21 KD1 (C, H, M) and Snx21 KD2 (D, I, N) salivary glands, fat tissue and midgut sections. Immunostaining of the early endosome marker Rab5 and the late endosome marker Rab7 revealed normal endosomal patterns in all cases. (E, F), (J, K), (O, P) Quantification of individual sizes of Rab5- or Rab7-positive structures represented in (B–D), (G–I) and (L–N), respectively. Kruskal-Wallis test with Dunn's multiple comparison test; mean ± SD. * means $P < 0.05$; ** means $P < 0.01$; *** means $P < 0.001$, **** means $P < 0.0001$. Scale bars represent 1 mm in panel (A) and 10 μm in panels (B–D), (G–I) and (L–N).

control. Importantly, GFP signal from the transgene was lost in prepupae coexpressing either one of two Snx21 knockdown constructs: *GD10120* or *KK10320* (Fig. 3A), referred to as Snx21 KD1 and Snx21 KD2 hereafter, respectively. This experiment shows that these Snx21 RNAi tools efficiently eliminate the Snx21 protein even if it is highly overexpressed via the UAS-Gal4 system. Interestingly, knockdown of Snx21 did not have an obvious effect on the size or distribution of Rab5- or Rab7-positive structures in larval tissues (Fig.3B–P). As such, Snx21 RNAi salivary gland (Fig. 3C,D), fat body (Fig. 3H,I) and midgut (Fig. 3M,n) cells all show largely normal endosomal patterns when compared to the corresponding controls (Fig.3B,G,L). Quantification revealed minor differences in endosomal size in some cases, most notably in fat tissue, where early endosomal size is increased in the case of the KD2 line, and late endosomes are also bigger than the control in the case of both KD lines (Fig. 3E,F,J,K,O,P). Averages of the measured sizes are very close to the control in each of these cases, though, and only a narrow size range accounts for the statistically significant differences. Based on this, we propose that while loss of Snx21 only has a minor effect on the overall pattern of endosomal compartments, its overexpression appears to significantly alter the organization of the endosomal system in Drosophila tissues.

Overexpression of Snx21 enhances endocytosis in a Flotillin2-dependent manner

Enlargement of late endosomes in Snx21 overexpressing cells is a common feature of all cell types that we investigated, and it may arise from (a) increased input from early endosomes or (b) decreased output toward lysosomes. In other words, overexpression of Snx21-GFP may (a) enhance the early steps of endocytosis or (b) negatively affect endosomal maturation/lysosomal trafficking. To differentiate between these possibilities and to investigate the dynamics of endosomal trafficking in Snx21 overexpressing cells, we analyzed endocytic flow in the highly endocytic garland nephrocytes where (similarly to other larval tissues) Snx21-GFP primarily colocalizes with late endosomes (Fig. 4A–C, J). The remarkably organized endosomal system of these podocyte-like cells is sensitive to genetic manipulations and represents an excellent model system to analyze the functions of proteins with presumable endosomal roles [40,41]. *Ex vivo* cultured nephrocytes take up and rapidly process fluorescently labeled endocytic tracers added to the medium [42–44]. We carried

© 2026 The Author(s). *The FEBS Journal* published by John Wiley & Sons Ltd on behalf of Federation of European Biochemical Societies.

17424658, 0, Downloaded from https://febs.onlinelibrary.wiley.com/doi/10.1111/febs.70618 by HUN-REN Biological Research Center, Szeged, Wiley Online Library on [25/11/2026]. See the Terms and Conditions (https://onlinelibrary.wiley.com/terms-and-conditions) on Wiley Online Library for rules of use; OA articles are governed by the applicable Creative Commons License

out pulse-chase experiments by allowing nephrocytes to internalize BSA-Alexa^{647} for 5 min (pulse), then imaged the cells after 45 min (chase) (Fig. 4D–I). Based on the literature, this time is enough for the tracer to traffic through the early and late endosomal compartments and fill up the so-called terminal lysosomal network of nephrocytes [42,45]. Accordingly, control cells contained numerous tracer-positive structures, the majority of which were also positive for Lysotracker Red (LTR), a vital dye that strongly accumulates in acidic lysosomes (Fig. 4D,M). The average size of BSA-positive structures in control cells was ~0.34 μm^2 (Fig. 4K), and based on our colocalization experiments, this size is indeed typical for lysosomes. Nephrocytes expressing Snx21-GFP also contain many LTR-BSA double-positive structures (Fig. 4g) indicating that acidic lysosomes are present and the terminal lysosomal network of these cells is accessible for the tracer, just as in the case of control cells. While colocalization of LTR and BSA was similar to the control (Fig. 4M), the average size of BSA-positive structures was significantly increased to ~0.69 μm^2 (Fig. 4K). Notably, Snx21-GFP-positive rings (primarily late endosomes based on our colocalization data) do not contain BSA (please see insets in Fig. 4G), indicating that the tracer already left this endosomal compartment along its route toward lysosomes during the chase period.

Based on these results, we hypothesized that lysosomes receive increased amount of endocytic cargo in Snx21 overexpressing cells. To test this more directly, we analyzed endocytic flux by knocking down Rab7 with or without Snx21 overexpression. In the absence of Rab7 function, endosomal flux is blocked because late endosomes cannot fuse with lysosomes and consequently, the tracer gets stuck in stalled and enlarged late endosomes [46–49]. Accordingly, knockdown of Rab7 in nephrocytes led to the formation of large, spherical late endosomes with an average size of ~0.94 μm^2 (Fig. 4E,K). As expected, no evident colocalization of BSA and LTR could be observed in these fusion-deficient cells (Fig. 4E,M). Instead, inner regions of Rab7 RNAi cells contained structures that showed strongly enhanced LTR signal intensity without BSA-content. These most probably represent 'aged' late endosomes that were generated earlier and accumulated acidity over time [42].

Strikingly, combination of Snx21 overexpression with Rab7 knockdown led to the formation of extremely large BSA-positive structures with an average size of ~1,39 μm^2 (Fig. 4H,K), which were not positive for LTR (Fig. 4M). This suggests that the size of Rab7-deficient stalled late endosomes further increases because they receive an extra load of endocytic cargo upon Snx21 overexpression. Notably, Snx21-GFP still decorates the membrane of these large, stalled, BSA-filled late endosomes (please see insets in Fig. 4H) in Rab7 RNAi cells, indicating that Snx21-GFP is recruited to endosomes independent of Rab7 activity.

To evaluate the kinetics of earlier steps of endocytosis, we applied 1-min pulse and imaged Snx21 overexpressing versus control nephrocytes after 10 and 15 min of chase (Fig. 5A–D). We quantified the amount of the tracer in the subcortical endosomal population, as during this relatively short chase it does not access the perinuclearly located lysosomes. In this experimental setup, excessive uptake manifests in an increase in tracer-covered area compared with control cells [44,50,51]. Compared to control nephrocytes (Fig. 5A,B), Snx21 overexpressing nephrocytes (Fig. 5C,D) contained significantly larger BSA-positive endosomes covering a markedly increased area of these cells (Fig. 5E,F). This result supports our model that the early steps of endocytic trafficking are facilitated by Snx21 overexpression.

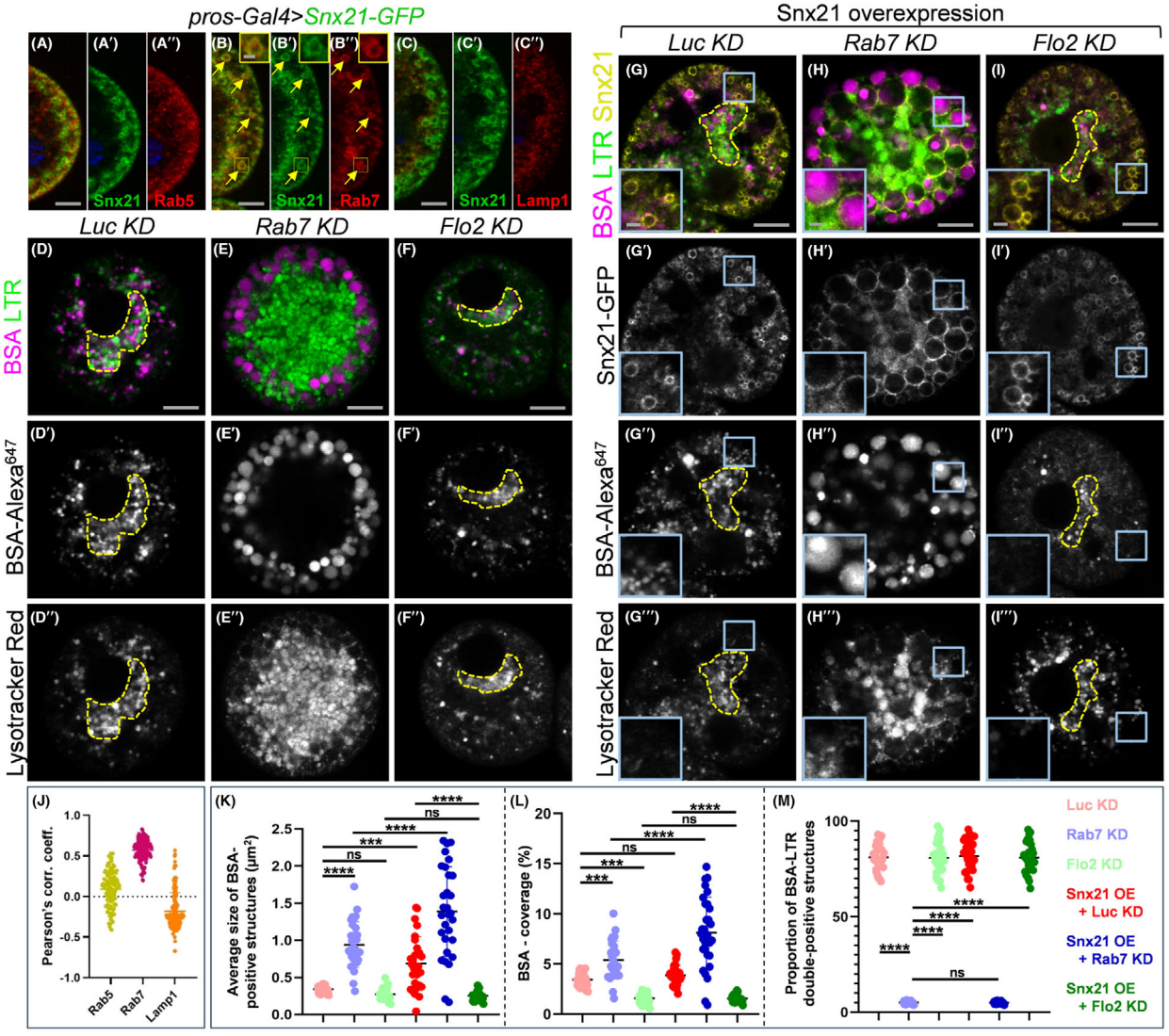
Notably, the pattern of LTR-positive vesicles in control and Snx21 overexpressing nephrocytes is similar to each other, and clearly different from the Rab7 knockdown case, where the LTR signal intensity is strongly increased (please compare Fig.4D",G" with Fig. 4E"). This is in line with normal lysosomal function in Snx21 overexpressing cells. To test this more directly, we added BSA-DQ^{Red} to the medium of cultured nephrocytes for a 5-min pulse period, followed by 1-h chase, allowing the tracer to reach lysosomes (Fig. 5G–I). Fluorescence of BSA-DQ^{Red} is quenched in its intact form, while its degradation by proteases leads to the formation of highly fluorescent products [44,52]. In control nephrocytes (Fig. 5G), fluorescence of BSA-DQ^{Red} can be detected in vesicles with variable sizes as well as in the cytosol, indicating that degradation products are generated and released from lysosomes. In contrast, inhibiting lysosomal delivery of the tracer by knocking down Rab7 (Fig. 5H) strongly decreases cytoplasmic green fluorescence. Here, BSA-DQ^{Red} can be subjected to only partial degradation (indicated by patches of the BSA-DQ^{Red} signal) without substantial release to the cytosol. This leads to a significantly higher vesicular versus cytosolic red fluorescence ratio in Rab7 knockdown cells compared with control nephrocytes. In the case of Snx21 overexpressing cells (Fig. 5I), the ratio of vesicular versus cytosolic fluorescence of BSA-DQ^{Red} does not differ significantly from the control (Fig. 5J), indicating efficient trafficking to digesting lysosomes. These results demonstrate that the

© 2026 The Author(s). *The FEBS Journal* published by John Wiley & Sons Ltd on behalf of Federation of European Biochemical Societies.

17424658, 0, Downloaded from https://febs.onlinelibrary.wiley.com/doi/10.1111/febs.70618 by HUN-REN Biological Research Center, Szeged, Wiley Online Library on [25/11/2026]. See the Terms and Conditions (https://onlinelibrary.wiley.com/terms-and-conditions) on Wiley Online Library for rules of use; OA articles are governed by the applicable Creative Commons License

enlarged lysosomes resulting from Snx21 overexpression are qualitatively different from those resulting from blocking the fusion of late endosomes with lysosomes by knocking down Rab7. Taken together, these results suggest that Snx21 overexpression facilitates the trafficking of endosomal cargo toward lysosomes.

It was recently shown that besides clathrin-mediated endocytosis, nephrocytes continuously exercise dynamin-independent endocytosis to maintain ultrafiltration filter permeability [53]. Here, Flo2 was identified as a novel key protein in the raft-mediated turnover of Nephrin, a defining component of the nephrocyte diaphragm. This study demonstrated that Flo2 knockdown cells show perturbed endocytic uptake of fluorescently labeled avidin because of altered filter permeability due to perturbed Nephrin trafficking. Using the same knockdown reagent, we carried out the above *ex vivo* experiment in Flo2 knockdown nephrocytes and in Flo2 knockdown nephrocytes that simultaneously overexpressed Snx21 to analyze whether the effect of Snx21 facilitating endocytosis in nephrocytes utilizes the Flo2-mediated pathway. In Flo2 knockdown cells, the average size of BSA-positive structures was only slightly decreased compared to the control cells (~0.27 μm^2 and ~ 0.34 μm^2, respectively) (Fig. 4F,K), although BSA-coverage was significantly decreased (Fig. 4L). The distribution of LTR-positive structures and their colocalization ratio with the tracer was similar to the control (Fig. 4M). These results indicate that Flo2



© 2026 The Author(s). *The FEBS Journal* published by John Wiley & Sons Ltd on behalf of Federation of European Biochemical Societies.

17424658, 0, Downloaded from https://febs.onlinelibrary.wiley.com/doi/10.1111/febs.70618 by HUN-REN Biological Research Center, Szeged, Wiley Online Library on [25/11/2026]. See the Terms and Conditions (https://onlinelibrary.wiley.com/terms-and-conditions) on Wiley Online Library for rules of use; OA articles are governed by the applicable Creative Commons License

Fig. 4. Snx21 enhances endocytosis in a Flotillin2-dependent manner. (A–C) Immunostainings for markers of different endolysosomal populations in Snx21-GFP expressing garland nephrocytes. Magnifications of the indicated area (yellow rectangle) are shown as insets in the upper right corners. Overlap (yellow arrows) of the Snx21-GFP and Rab7 signals in ring-like structures shows the predominantly late endosomal localization of Snx21. (D–I) Pulse-chase experiments using *ex vivo* cultured nephrocytes using BSA-Alexa^{647} (BSA—pseudocoloured to magenta) and costained with Lysotracker Red (LTR—pseudocoloured to green) to stain acidic structures. After the applied 5-min pulse followed by a 45-min chase, the terminal lysosomal network of control cells (D) contains numerous tracer-positive structures. Knockdown of Rab7 (E) leads to the formation of large, spherical late endosomes with no LTR signal, indicating that the tracer gets stuck in stalled late endosomes that are unable to fuse with lysosomes in the absence of Rab7 function. Nephrocytes expressing Snx21-GFP (G) also contain enlarged BSA-positive structures. Combination of Snx21 overexpression with Rab7 knockdown (H) leads to the formation of extremely large BSA-positive structures indicating that the size of Rab7-deficient, stalled late endosomes further increases because they receive more endocytic cargo as a result of Snx21 overexpression. In Flo2 knockdown nephrocytes (F), the average size of BSA-positive structures is similar to that of the control cells. However, the BSA coverage decreases, indicating that Flo2 RNAi cells take up less tracer even though its intracellular trafficking is not impaired. Knocking down Flo2 in Snx21 overexpressing cells (I) restores the average size of BSA-positive structures to that seen in controls, with a BSA coverage similar to that of Flo2 knockdown alone, demonstrating that Snx21 acts in a Flo2-dependent manner. Perinuclear regions encircled with yellow dashed lines highlight the overlap of BSA and LTR in the terminal lysosomal network of nephrocytes that have normal Rab7 function. Magnifications of the indicated areas (blue rectangles) of Snx21-GFP-expressing cells are shown as insets in the lower left corners. (J) Quantification of Pearson's correlation coefficients (mean ± SD) of Snx21-GFP and endolysosomal markers in nephrocytes represented in (A–C). (K and L) Quantification of the average size and coverage of BSA-positive structures in nephrocytes represented in (d–i). Sidak's multiple comparison tests; mean ± SD. (M) Quantification of the ratio of BSA-LTR double-positive structures in nephrocytes represented in (D–I). Kruskal-Wallis test with Dunn's multiple comparison test; mean ± SD. * means $P < 0.05$; ** means $P < 0.01$; *** means $P < 0.001$, **** means $P < 0.0001$. Scale bars represent 5 μm and 1 μm (insets).

knockdown cells take up less tracer, while its intracellular trafficking is not impaired. Importantly, knocking down Flo2 in Snx21 overexpressing cells (Fig. 4I) restored the average size of BSA-positive structures to the control range (from ~0.69 μm^2 to ~0.25 μm^2) (Fig. 4K) with a BSA coverage and LTR pattern similar to that of Flo2 knockdown alone (Fig. 4L,M). This result demonstrates that Snx21 overexpression exerts its effect in a Flo2-dependent manner and points to the role of Snx21 in flotillin-mediated endocytosis, which probably affects ultrafiltration barrier integrity that indirectly influences BSA uptake. We thus propose that Snx21 facilitates endosomal flux toward late endosomes/lysosomes in a Flo2-dependent manner.

Snx21 physically and functionally interacts with flotillins

Next, we aimed to investigate this novel Snx21-flotillin interaction further. For this purpose, we established new UAS-Flo1-10xHA and UAS-Flo2-3xFLAG transgenic stocks and used them in coimmunoprecipitation and colocalization experiments. For coimmunoprecipitations, either Snx21-GFP alone, or Flo1-10xHA with Flo2-3xFLAG, or Snx21-GFP with Flo10x-HA and Flo2-3xFLAG were (co)expressed using the tubulin-Gal4 driver and whole animal lysates were subjected to immunoprecipitation with anti-FLAG beads (Fig. 6A). Analysis of the total lysates by either a-GFP, a-HA, or a-FLAG antibodies showed the presence of all three proteins as single bands at the expected molecular weights. Flo2-3xFLAG efficiently retrieved Flo1-10xHA, as expected based on the known existence of Flo1-Flo2 oligomers. Importantly, Snx21-GFP was also detected on a-FLAG beads in the presence of flotillins, indicating their *in vivo* interaction.

We next turned to the larval wing imaginal disk for the investigation of the Snx21-flotillin interaction in a cellular environment, as earlier studies focused on flotillin function during the development of this tissue [54,55]. First, we wanted to check the colocalization of Snx21 and our flotillin reporters in the wing disks of third-instar larvae. As expected, the Flo1-10xHA and Flo2-3xFLAG reporters reasonably well-colocalized with each other, and they were primarily found at the plasma membrane of wing disk cells (Fig. 6B). We did not see these flotillins in intracellular structures, and no colocalization with late endosomal Rab7 could be observed (Fig. 6C). Strikingly, when coexpressed with Snx21-GFP, the distribution of flotillin reporters became more vesicular, suggesting that in Snx21 overexpressing cells, more flotillins enter the endosomal system because of the endocytosis-promoting effect of Snx21. Colocalization of Snx21-GFP with Flo1-10xHA and endogenous Rab7 on late endosomes (Fig. 6D, arrowheads) or with Flo1-10xHA and Flo2-3xFLAG in wing disk cells and other larval tissues (Fig. 6E–H, arrowheads) also indicates the interaction between Snx21 and flotillins in the endosomal system.

© 2026 The Author(s). *The FEBS Journal* published by John Wiley & Sons Ltd on behalf of Federation of European Biochemical Societies.

17424658, 0, Downloaded from https://febs.onlinelibrary.wiley.com/doi/10.1111/febs.70618 by HUN-REN Biological Research Center, Szeged, Wiley Online Library on [25/11/2026]. See the Terms and Conditions (https://onlinelibrary.wiley.com/terms-and-conditions) on Wiley Online Library for rules of use; OA articles are governed by the applicable Creative Commons License

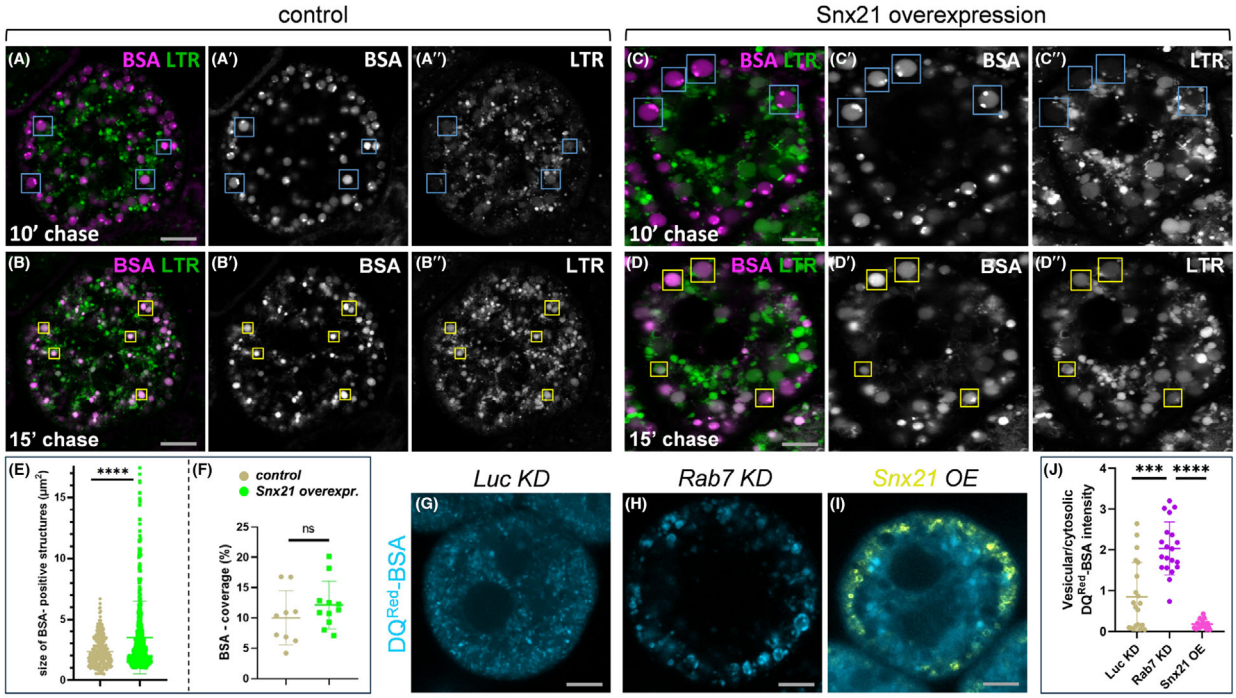


Fig. 5. Snx21 facilitates endocytic trafficking in nephrocytes without impairing lysosomal function. (A–D) *Ex vivo* cultured control and Snx21-GFP (GFP signal not shown) expressing nephrocytes containing endocytosed BSA-Alexa^{647} (BSA—pseudocoloured to magenta) and costained with Lysotracker Red (LTR—pseudocoloured to green) to stain acidic structures. Nephrocytes were allowed to take up BSA for 1 min (pulse) and imaged after the indicated times (chase). Colocalization of the tracer with faint LTR signal can already be detected after 10 min (blue rectangles) in both genotypes (A and c). BSA-positive structures show intensive tubulation and enhanced LTR intensity after 15 min (yellow rectangles), indicating that the tracer reaches the terminal lysosomal network in both genotypes (B and D). (E) Quantification of the size of BSA-positive structures in nephrocytes represented in (A and C). Mann–Whitney *U* test; mean ± SD. (F) Quantification of BSA-coverage in nephrocytes represented in (A and C). Mann–Whitney *U* test; mean ± SD. (G–I) Pulse-chase labeling of nephrocytes using DQ^{Red}-BSA (pseudocoloured to light blue). After a 5-min pulse, followed by a 1-h chase, the detected signal represents dequenched, fluorescent products of DQ^{Red}-BSA. Dequenching is observed only in patches within enlarged vesicles in Rab7 knockdown nephrocytes due to a block of endocytic progression (H), while the signal appears both in vesicles and in the cytosol in control (G) and Snx21-GFP (pseudocoloured to yellow) expressing cells (I), indicating that degradation of the tracer is followed by its release to the cytosol. (j) Quantification of vesicular/cytosolic DQ^{Red}-BSA intensities in nephrocytes represented in (g–i). Kruskal-Wallis test with Dunn's multiple comparison test; mean ± SD. * means $P < 0.05$; ** means $P < 0.01$; *** means $P < 0.001$, **** means $P < 0.0001$. Scale bars represent 5 µm.

We detected relatively frequent colocalization of Snx21-GFP with flotillins in wing disks (Fig. 6E), salivary glands (Fig. 6F) and in the midgut (Fig. 6G), while colocalization events were rare in the fat tissue (Fig. 6H). Surprisingly, we could not detect obvious colocalization of the reporters in nephrocytes (Fig. 6I). Nonetheless, these results support the *in vivo* interaction of Snx21 and flotillins.

Changes in flotillin levels have been shown to affect Wingless (Wg) and Hedgehog (Hh) secretion and uptake in the developing wing disk [54,55], so we used this tissue to test the functional interaction between Snx21 and flotillins. Specifically, we focused on the intracellular trafficking of Wg via a genetic mosaic approach as a sensitive method that enables the detection of even subtle changes and excludes animal-to-animal variability. We used the engrailed-Gal4 driver to express UAS-driven transgenic constructs in the posterior half of the wing disk (labeled by RFP coexpression) and compared Wg levels within the morphogen-producing cells of this half to those that are located in the nonexpressing anterior half of the wing disk. As similar results were reported by the expression of Flo2 alone or coexpression of Flo1 and Flo2 [54,55], we analyzed the effects of Flo2-3xFLAG expression in our experiments. Importantly, the Wg-covered area (as well as the signal intensity) was markedly increased in the case of Flo2 overexpression (Fig. 7A,M). This is in line with the findings of Katanaev *et al.*, who already showed that Flo2

© 2026 The Author(s). *The FEBS Journal* published by John Wiley & Sons Ltd on behalf of Federation of European Biochemical Societies.

17424658, 0, Downloaded from https://febs.onlinelibrary.wiley.com/doi/10.1111/febs.70618 by HUN-REN Biological Research Center, Szeged, Wiley Online Library on [25/11/2026]. See the Terms and Conditions (https://onlinelibrary.wiley.com/terms-and-conditions) on Wiley Online Library for rules of use; OA articles are governed by the applicable Creative Commons License

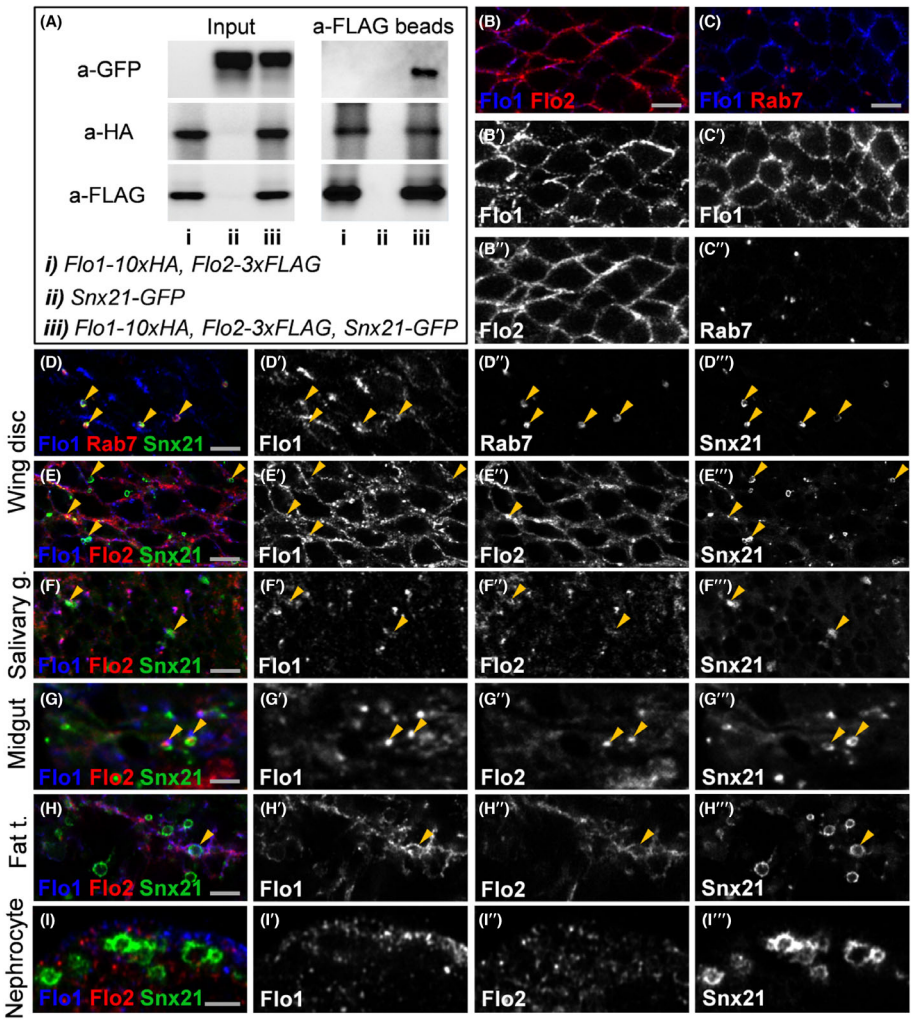


Fig. 6. Snx21 coimmunoprecipitates and colocalizes with flotillins. (A) Coimmunoprecipitation of whole animal lysates using anti-FLAG beads. Either Snx21-GFP alone (ii), or Flo1-10xHA with Flo2-3xFLAG (i), or Snx21-GFP with Flo10x-HA and Flo2-3xFLAG (iii) are (co) expressed using the ubiquitous tub-Gal4 driver. Snx21-GFP is detected on a-FLAG beads only in the presence of flotillins, indicating their *in vivo* interaction. Representative images of three independent experiments, all with similar results. (B–I) Colocalization analysis of Snx21 and the Flo1-10xHA and Flo2-3xFLAG reporters in tissues of third instar larvae. Flo1-10xHA and Flo2-3xFLAG reporters colocalize well, primarily at the plasma membrane (B) and Flo1 shows no overlap with late endosomal Rab7 in wing disk cells (C). In contrast, when coexpressed with Snx21-GFP, the distribution of flotillins becomes more vesicular, especially in the case of Flo1 (D′ and E′). Colocalization of Snx21-GFP with Flo1-10xHA and endogenous Rab7 on late endosomes (D, arrowheads) or with Flo1-10xHA and Flo2-3xFLAG (E–H, arrowheads) supports the interaction between Snx21 and flotillins in the endosomal system of multiple cell types. Representative images of two independent experiments, both with similar results. Scale bars represent 5 μm.

overexpression enhances the endocytosis of Wg [55]. The combination of Luc KD (used as control) with Flo2 overexpression also seemed to slightly decrease the Wg signal, although the change was not statistically significant compared to the effect of Flo2 overexpression alone (Fig. 7C,M). There was also a tendency toward decreased amounts of Wg in the producing cells in the case of both Snx21 knockdown constructs (Fig. 7E,G), which was again not statistically significant compared to the control case (Fig. 7M). Of note, when we overexpressed Flo2 on a Snx21 RNAi background (Fig. 7I,K), the Flo2 overexpression-induced accumulation of Wg was diminished and Wg-producing cells showed intracellular Wg amounts similar to that of Snx21 knockdown alone (Fig. 7M). These results suggest that the effect of Flo2 overexpression on the intracellular accumulation of Wg depends on Snx21.

© 2026 The Author(s). *The FEBS Journal* published by John Wiley & Sons Ltd on behalf of Federation of European Biochemical Societies.

17424658, 0, Downloaded from https://febs.onlinelibrary.wiley.com/doi/10.1111/febs.70618 by HUN-REN Biological Research Center, Szeged, Wiley Online Library on [25/11/2026]. See the Terms and Conditions (https://onlinelibrary.wiley.com/terms-and-conditions) on Wiley Online Library for rules of use; OA articles are governed by the applicable Creative Commons License

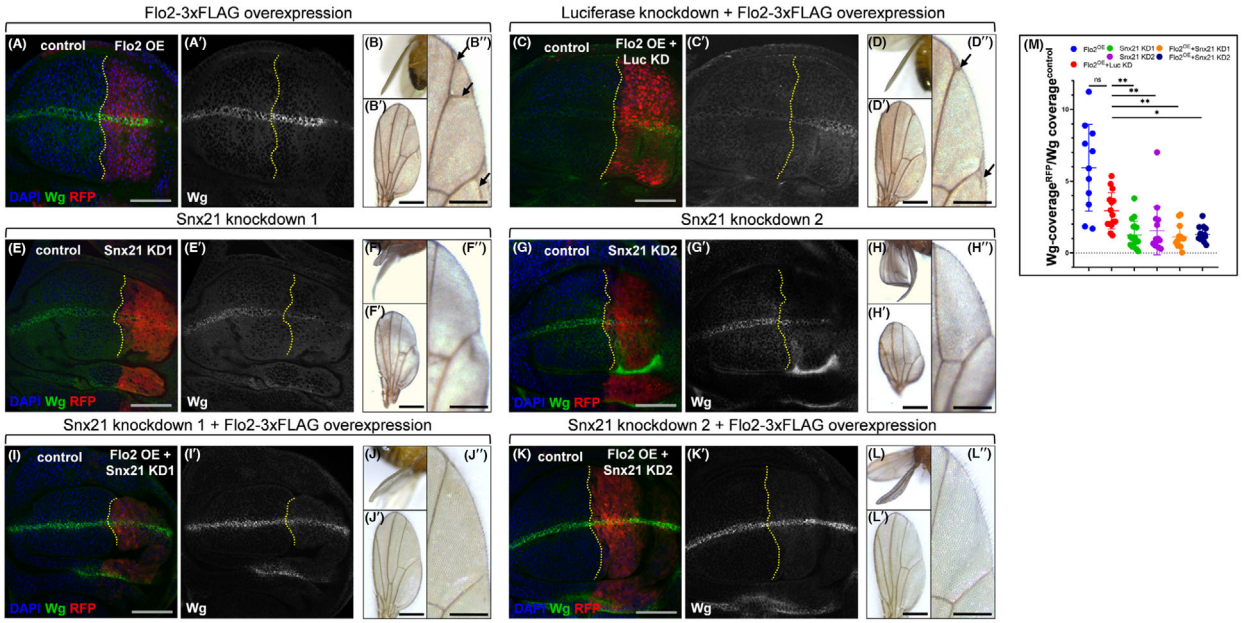


Fig. 7. Snx21 functionally interacts with flotillins. (A, C, E, G, I, and K) Immunostaining of endogenous Wg in the wing disks of third instar larvae. Engrailed-Gal4 drives the expression of UAS-driven transgenes in the posterior half of wing disks (labeled by RFP coexpression). The border of the anterior and posterior half of the wing disks is indicated by yellow dashed lines. Wg signal within Wg-producing cells in the posterior half of the analyzed wing disks is markedly increased in the case of Flo2 overexpression alone (A) or in combination with Luciferase (control) knockdown (C). The Wg signal seems slightly decreased in the case of Snx21 RNAi knockdowns (E and G). When Flo2 is overexpressed together with Snx21 RNAi (I and K), the amount of intracellular Wg is similar to that of Snx21 knockdown alone, indicating that the Flo2 overexpression-dependent increase of Wg requires Snx21. (B, D, F, H, J and L) Wing morphology of young male flies expressing the indicated transgenic constructs in the dorsal half of the developing wing (driven by MS1096-Gal4). Flo2 overexpression alone (B) or in combination with Luciferase knockdown (D) leads to the formation of extra wing veins: bifurcations appear most frequently in the distal regions of the longitudinal L4 and L5 veins (arrows), while wing blades remain straight. In contrast, expression of Snx21 KD1 (F) or KD2 (H) results in the formation of curled wings, but these do not affect the normal patterning of wing veins. Strikingly, coexpression of Snx21 KD1 (J) or Snx21 KD2 (L) completely suppresses the formation of extra wing veins caused by Flo2-3xFLAG overexpression. (M) Quantification of Wg within Wg-producing cells in wing disks represented in (A, C, E, G, I and K). Kruskal-Wallis test with Dunn's multiple comparison test; mean ± SD. * means $P < 0.05$; ** means $P < 0.01$; *** means $P < 0.001$, **** means $P < 0.0001$. Scale bars represent 10 μm in (a, c, e, g, i and k), 0.5 mm in (B′, D′, F′, H′, J′ and L′) and 0.25 mm in (B", D", F", H", J" and L").

Finally, to extend our genetic interaction experiments to the adult wing, we used the MS1096-Gal4 driver for the overexpression of UAS-driven transgenes in the dorsal half of the developing wing and analyzed the wing morphology of young adult male flies. Control flies expressing Luc KD showed wild-type wing morphology (Fig. S2A) without any visible abnormalities, including normal vein patterning (Fig. S2A") and straight wing blades. MS1096-Gal4-mediated overexpression of Flo2-3xFLAG alone (Fig. 7B) or combined with Luc KD (Fig. 7D) resulted in the formation of extra wing veins visible as bifurcations appearing most frequently in the distal regions of the longitudinal L4 and L5 veins (Fig. 7B,D", arrows). These abnormalities were detected in 95% of the F1 progeny, while other aspects of wing morphology were normal, including straight wing blades. Importantly, expression of the previously published [54], untagged UAS-Flo2 transgene or coexpression of untagged Flo2 and Flo1 produced the same extra wing vein phenotype (Fig. S2B,C). Expression of the Snx21 KD1 or KD2 constructs resulted in the formation of curled wings in 90% and 100% of the F1 progeny, respectively, without any other major defects of wing morphology (Fig. 7F,H). Notably, the patterning of wing veins was similar to the control in both cases (Fig. 7F",H"). Importantly, knocking down Snx21 by either UAS-KD1 or -KD2 on a Flo2-3xFLAG overexpressing background (Fig. 7J,L) prevented the formation of extra veins (Fig. 7J",L"), which indicates that Snx21 is required for the appearance of this Flo2 overexpression-dependent phenotype. These results further support the functional interaction of these proteins. In summary, our results show that Snx21 and

© 2026 The Author(s). *The FEBS Journal* published by John Wiley & Sons Ltd on behalf of Federation of European Biochemical Societies.

17424658, 0, Downloaded from https://febs.onlinelibrary.wiley.com/doi/10.1111/febs.70618 by HUN-REN Biological Research Center, Szeged, Wiley Online Library on [25/11/2026]. See the Terms and Conditions (https://onlinelibrary.wiley.com/terms-and-conditions) on Wiley Online Library for rules of use; OA articles are governed by the applicable Creative Commons License

flotillins both physically and functionally interact with each other in the context of Flotillin-mediated endocytosis in Drosophila.

Discussion

In this study, we provide the first experimental evidence for the molecular function of Drosophila Snx21 and characterize its role as a potential novel positive regulator of flotillin-mediated endocytosis. We demonstrate that Snx21 localizes and functions in the endosomal system, and provide biochemical, microscopy-, and genetic interaction-based evidence supporting the Snx21-flotillin interaction in multiple fruit fly tissues.

Localization of Snx21 in the endosomal system and its effect on endosomal trafficking is in line with earlier studies [30,31]. We found that Drosophila Snx21 primarily localizes to Rab7-positive late endosomes, and in most of the investigated tissues, we could not detect its significant enrichment on Rab5-positive early endosomes. This is a bit surprising in the light of our *in vitro* results that show the preference of Snx21 toward PI(3)P and no obvious interaction with the late endosome-enriched PI(3,5)P_2. These findings can be resolved if we assume that besides its lipid-binding PX-domain, other parts (e.g., the PXB-domain) of the protein also influence the localization of Snx21 via binding to certain proteins on late endosomes (coincidence detection). These nonphospholipid interactions likely contribute to the localization of Snx21 in an *in vivo* context where other factors of the endosomal maturation machinery are all present. Notably, our nephrocyte data show that Snx21-GFP decorates tracer-positive endosomes even in the absence of late endosomal Rab7 function. This indicates that Snx21 is recruited to endosomal membranes prior to Rab7 activity and suggests that other proteins of the endosomal maturation cascade play an important role in the localization of Snx21 to endosomes. In fact, Snx21 might be recruited to endosomal membranes with a composition representing an earlier stage of maturation, for example, endosomes in the early-to-late transition state, which is in line with its strong binding to PI(3)P.

Of note, we find that excess Snx21 perturbs normal endocytic trafficking. Depending on the cell type, various compartments of the endosomal system expand upon Snx21 overexpression, with the common and most prominent effect on late endosomes. One possible explanation for the presence of enlarged late endosomes would be a defect of endosomal maturation, when endocytic flux is blocked—just like in the case of Rab7 knockdown. In this scenario, high amounts of Snx21 would have an inhibitory effect on the recruitment of endosomal regulatory proteins (e.g., fusion factors) leading to the appearance of stalled late endosomes. However, our nephrocyte results based on different experimental setups all support that lysosomal function is not compromised and endocytic trafficking is unimpeded in Snx21-overexpressing nephrocytes. Thus, increased trafficking toward late endosomes is the most likely cause of the enlargement of late endosomes in Snx21-overexpressing cells instead of an endosomal maturation defect.

Using nephrocytes with naturally high endocytic activity, we provide evidence that overexpressed Snx21 exerts its effect on the endosomal system in a Flo2-dependent manner. Flotillin-mediated endocytosis is required for the turnover of the diaphragm protein Nephrin and loss of Flo2 function leads to altered filtration characteristics and to impaired endocytosis [53]. Flotillins induce membrane deformation upon their association with lipid rafts and, as a result, vesicles can bud from the donor membrane [56]. In line with this, an excess amount of flotillins leads to the formation of plasma membrane invaginations and the accumulation of intracellular vesicles [57]. In Drosophila, flotillin overexpressing eye imaginal disks accumulate multivesicular bodies containing cell adhesion molecules of the Ig superfamily [54] and endocytosis of the Wg morphogen is also enhanced upon flotillin overexpression in the wing disk [55]. We show here that Snx21 knockdown reverses Wg accumulation upon flotillin overexpression in the wing disk. Further supporting the novel finding that Snx21 and flotillins cooperate in the endosomal system, we find that Snx21 coimmunoprecipitates and colocalizes with flotillins *in vivo*. Surprisingly, we could not detect evident colocalization between our Snx21 and flotillin reporters in these cells. As a possible explanation for the apparent lack of such colocalization, one might hypothesize that the Snx21-flotillin interaction is only transient in the highly endocytic nephrocytes that exercise continuous, intensive endocytic trafficking, combined with our assumption that most of the flotillin proteins are presumably associated with the ultrafiltration diaphragm, so their endosomal pool might be very low in these cells. Thus, the overlap between Snx21 and flotillins might be extremely hard to catch in our fixed nephrocyte samples. Based on all these data, we identify Snx21 as a potential novel positive regulator of flotillin-mediated endocytosis.

Interestingly, we could not detect any major changes in the endosomal system of Snx21 loss-of-function cells, while Snx21 overexpression leads to alterations of the endosomal network in various Drosophila

© 2026 The Author(s). *The FEBS Journal* published by John Wiley & Sons Ltd on behalf of Federation of European Biochemical Societies.

17424658, 0, Downloaded from https://febs.onlinelibrary.wiley.com/doi/10.1111/febs.70618 by HUN-REN Biological Research Center, Szeged, Wiley Online Library on [25/11/2026]. See the Terms and Conditions (https://onlinelibrary.wiley.com/terms-and-conditions) on Wiley Online Library for rules of use; OA articles are governed by the applicable Creative Commons License

tissues. Similarly, loss of flotillin function in Drosophila also fails to produce severe phenotypes as the *flo2* null mutant (that simultaneously disrupts Flo1 function as well) is viable with no major defects. Given that flotillin overexpression also leads to clear alterations, its behavior is quite similar to that of Snx21. As a possible explanation, one can think of a potential redundancy/compensation among Snx family members, just like it was proposed in the case of flotillins and other SPFH-domain containing proteins [12]. Such compensation is less straightforward in the case of Snx21, though, because no other PXB-domain containing Snx protein exists in Drosophila. A more likely explanation is a narrow tissue and/or cellular pathway-specificity of Snx21 that involves only a subset of tissues/developmental stages. As we identify Snx21 as a novel functional partner of flotillins, the specificity of the flotillin-mediated endocytic pathway toward certain cargo molecules supports this idea. Indeed, the effect of flotillin overexpression seems to be specific for igCAMs such as Rst, Kirre, and Sns, but not for DE-Cadherin in the eye imaginal disk [54]. Similarly, trafficking of Wg and Hh, but not Dpp, is perturbed in flotillin overexpressing wing disks [55]. Based on these and our results, we propose that the function of Snx21 is specific for flotillin-mediated trafficking in Drosophila.

An important known example of a close cooperation between an Snx protein and flotillins was demonstrated in HeLa cells [58]. Here, flotillins interact with SNX4 and Rab11a to regulate the sorting and recycling of the transferrin receptor and E-cadherin from the tubulovesicular recycling compartment toward the plasma membrane. In this context, the membrane deforming properties of flotillins and the BAR domain of SNX4 might be coordinated to enable efficient tubule formation. As Snx21 does not have a BAR domain, a similar mechanism seems unlikely in our case. Instead, Snx21 may recruit further effector proteins such as septins to support the formation/stabilization of tubules emanating from the endosomal surface. This hypothesis agrees with the finding of Danson and colleagues who showed that overexpressed Snx21 recruits endogenous septins to the surface of endosomes [31]. Based on the well-established role of septin filaments in membrane remodeling [59–62], investigating the involvement of septins in the aspect of Snx21-flotillin interaction could represent an exciting future follow-up for the present study.

As upregulation of flotillins is involved in the pathogenesis of a multitude of diseases including cancer, diabetes, neurodegenerative and other neurological disorders, cardiomyopathy and infectious diseases [25], identification of novel interactors of flotillin-mediated trafficking adds important new details to our understanding of flotillin function in disease. Specifically, upregulation of flotillins leads to altered cellular adhesion and contributes to tumorigenesis as well as to the development of neurodegenerative diseases [24]. Our identification of Snx21 as a novel interaction partner of flotillins and its requirement for the effects of flotillin overexpression is thus key for understanding their mechanisms of action in health and disease.

Materials and methods

Molecular cloning

ESTs were obtained from the Drosophila Genomics Resource Center (DGRC, NIH Grant 2P40OD010949). For GFP- or GST-tagging, the coding region of Drosophila Snx21 was amplified using the #LD12265 clone (DGRC Stock 3702; https://dgrc.bio.indiana.edu//stock/3702; RRID: DGRC_3702) as a template. To get UAS-GFP-Snx21, we used the following primers (for: ATGCGC GGCCGCAATGCCCATTCACGCCGTGAT; rev: ATGC GGTACCTCAAATTGTTTC-AGTGCGAGGATCGATC TT) and subcloned the resulting product in the pACU-KEGFP (modified pACU) vector as a NotI-Acc65I fragment. To get UAS-Snx21-GFP, we applied Gibson assembly using the pACU-KEGFP vector and the following primers (for: TTATTGAATACAAGAAGAGAACTCTG AATAGGGAATTGGGATGCCCATTCACGCCGTGAT; rev: CCCCGGTGAACAGCTCCTCGCCCTTGCTCA CC ATTTTGTGAATTGTTTCAGT-GCGAGGAT). To get GST-Snx21 we used the following primers (for: ATGCAG ATCTAT-GCCCATTCACGCCGTGAT; rev: ATG CCTCGAGAATTGTTTCAGTGCGAGGATCGATCTT) and subcloned the resulting product in the pETARA expression vector as a BglII-XhoI fragment. For 10xHA-tagging, the coding region of Drosophila Flo1 was amplified using the #SD10657 clone (DGRC Stock 3112; https://dgrc.bio.indiana.edu//stock/3112; RRID: DGRC_3112) as a template. To get UAS-Flo1-10xHA we used the following primers (for: TATCACGAATTCCATG- ACTT GGGGATTTGTAACCTGC; rev: CCAATTGGTACCGC CAGC-ATGCACAGACCGAG) and subcloned the resulting product in the pACU-10xHA vector (modified pACU) as an EcoRI-Acc65I fragment. For 3xFLAG-tagging, the coding region of Drosophila Flo2 was amplified using the #RE74011 clone (DGRC Stock 10 061; https://dgrc.bio.indiana.edu//stock/10061; RRID: DGRC_10 061) as a template. To get UAS-Flo2-3xFLAG we used the following primers (for: TATCACGAATTCATGGGCAACATA CACA-CGACGGGT; rev: CCAATTGGTACCCGCCT-TGGCCCCCGGTATCT) and subcloned the resulting product in the pACU-3xFLAG vector (modified pACU) as an EcoRI-Acc65I fragment.

© 2026 The Author(s). *The FEBS Journal* published by John Wiley & Sons Ltd on behalf of Federation of European Biochemical Societies.

17424658, 0, Downloaded from https://febs.onlinelibrary.wiley.com/doi/10.1111/febs.70618 by HUN-REN Biological Research Center, Szeged, Wiley Online Library on [25/11/2026]. See the Terms and Conditions (https://onlinelibrary.wiley.com/terms-and-conditions) on Wiley Online Library for rules of use; OA articles are governed by the applicable Creative Commons License

GST- fusion protein expression and purification

We expressed the recombinant GST-Snx21 protein in *E. coli* BL21(DE3) Rosetta cells. Protein expression was induced with 0.1 mM IPTG at 13°C overnight. Following expression, the cells were harvested and lysed. The recombinant protein was purified from the cytosolic fraction using glutathione affinity chromatography with glutathione Sepharose beads, as previously described [63]. The eluted protein was concentrated using a 30-kD pore size filter (Merck Millipore). Protein concentration was determined by a Bradford assay (Thermo Scientific #XG343066), and its purity and molecular weight were confirmed by sodium dodecyl sulfate/polyacrylamide gel electrophoresis (SDS/PAGE).

Liposome flotation assay

Liposomes were generated from synthetic lipids all purchased from Avanti Polar lipids in the following ratios: 10% POPE +90% POPC, 10% POPE +80% POPC +10% PI(3)P, 10% POPE +80% POPC +10% PI(3,5)P_2, 10% POPE +80% POPC +10% PI(3,4)P_2, 10% POPE +80% POPC +10% PI(3,4,5)P_3. POPE/PE (850757P): 1-palmitoyl-2-oleoyl-sn-glycero-3-phosphoethanolamine; PC/POPC (850457P): 1-palmitoyl-2-oleoyl-glycero-3-phosphocholine; PI(3)P (850154P): 1,2-dioleoyl-sn- glycero-3-phospho-(1′-myo-inositol-3′ – phosphate); PI(3,5)P2 (850154P): 1,2-dioleoyl-sn-glycero-3-phospho-(1′-myo-inositol-3′,5′-bisphosphate); PI(3,4)P_2 (850153P): 1,2-dioleoyl-sn-glycero-3-phospho-(1′-myo-inositol-3′,4′-bisphosphate); PI(3,4,5)P_3 (8501561): 2-dioleoyl-sn-glycero-3-phospho-(1′-myo-inositol-3′,4′,5′-trisphosphate). Lipid stocks were mixed in chloroform, which were then removed by evaporation under an inert nitrogen gas stream, followed by desiccation under vacuum. The dried lipid film was rehydrated in liposome generation buffer (20 mM HEPES, 100 mM NaCl, pH 7.4) to a final concentration of 10 mg·mL^{-1}. To form homogeneous liposomes, the lipid mixture was subjected to several rounds of sonication (2 × 1 min in a water bath sonicator) and vortexing (2 × 1 min), with brief incubations in a water bath near the lipids' phase transition temperature. Finally, the lipid emulsion was passed through a mini extruder fitted with a 100-nm pore size polycarbonate filter (Avanti Polar Lipids) 11 times to produce a population of unilamellar liposomes. These liposomes were used immediately for the flotation assay. The detailed protocol for the liposome flotation assay has been previously described [63]. In brief, the recombinant protein was incubated with the liposomes and then loaded onto a sucrose gradient. The samples were then centrifuged at 70 000 × ***g*** for 4 h at 4 °C. Following centrifugation, 12 one-milliliter fractions were collected from top to bottom. The protein in each fraction was precipitated with 100% trichloroacetic acid (TCA), dissolved in 45 µL of 2× Laemmli buffer, and boiled for 10 min before being validated by immunoblot. Each experiment was performed independently at least three times.

Immunoblotting of flotation assay fractions

Proteins precipitated by TCA were separated using 10% denaturing SDS/PAGE and then transferred for western blotting as previously described [64]. We used a rabbit polyclonal anti-GST antibody (Invitrogen, #A-5800) at a dilution of 1 : 3000 to detect the recombinant protein. A species-specific fluorescent secondary antibody (Li-COR #926–68 071) at a 1 : 7500 dilution was used for detection with a Li-COR Odyssey CLx laser scanner.

Coimmunoprecipitation

Approximately 200 mg adult flies of either the *+; tub-Gal4 / +; UAS-Snx21-GFP* or *+; tub-Gal4 / UAS-Flo1-10xHA; UAS-Flo2-3xFLAG* or *+; tub-Gal4, UAS-Snx21-GFP / UAS-Flo1-10xHA; UAS-Flo2-3xFLAG* genotypes were dounce homogenized in 2 mL of LBW buffer (lysis, binding, and wash: 1× PBS, 0.2% Triton X-100). Extracts were clarified by repeated centrifugation, taking care to leave as much of the upper fatty layer of the lysate behind as possible at each step. Extracts were further clarified by letting them pass through 300-µl Sephadex-G100 packed into disposable plastic columns by gravity flow. Extracts (750 µL) were incubated with 25 µL anti-FLAG magnetic beads (Pierce #36797) for 4 h, washed extensively, and eluted using nonreducing SDS sample buffer. Bound material and input lysates were separated on 10% SDS/PAGE and transferred onto a nitrocellulose membrane. The following antibodies were used for detection: Flo1-10xHA by anti-HA-HRP (Roche #12013819001), Flo2-3xFLAG by anti-Flag M2 (Sigma #F1804) and anti-mouse HRP (DAKO #P0447), and Snx21-GFP by anti-GFP (Invitrogen #A11122) and anti-rabbit HRP (DAKO #P0399). Blots were developed using ECL Prime reagent (Cytiva #RPN2232), and signals were detected using Uvitec's Alliance Q9.

Drosophila strains and genetics

All procedures were conducted in strict accordance with the 'Guide for the Care and Use of Laboratory Animals' and designed to minimize suffering, utilizing appropriate anesthesia and analgesia where necessary. Flies were raised on standard yeast/cornmeal/agar media at room temperature (RT). The UAS-GFP-Snx21, UAS-Snx21-GFP, UAS-Flo1-10xHA, and UAS-Flo2-3xFLAG lines were established by the HUN-REN BRC Drosophila Injection Facility, Szeged, Hungary. Further fly stocks used in this study were obtained from the Bloomington Drosophila Stock Center (BDSC) or from the Vienna Drosophila Resource Center (VDRC) and were the following: Luciferase RNAi

© 2026 The Author(s). *The FEBS Journal* published by John Wiley & Sons Ltd on behalf of Federation of European Biochemical Societies.

17424658, 0, Downloaded from https://febs.onlinelibrary.wiley.com/doi/10.1111/febs.70618 by HUN-REN Biological Research Center, Szeged, Wiley Online Library on [25/11/2026]. See the Terms and Conditions (https://onlinelibrary.wiley.com/terms-and-conditions) on Wiley Online Library for rules of use; OA articles are governed by the applicable Creative Commons License

(control) [BDSC #35788], Snx21 RNAi 1 [VDRC #25630], Snx21 RNAi 2 [VDRC #109618], Flo2 RNAi [VDRC #330316], Rab7 RNAi [BDSC #27051], MS1096-Gal4 [BDSC #8860], engrailed-Gal4, UAS-RFP [BDSC #30557], tubulin-Gal4 [BDSC #5138]. The prospero-Gal4 driver was obtained from [65]. The UAS-Flo2 and UAS-Flo2; UAS-Flo1 stocks were kindly provided by Vladimir Katanaev [54]. Standard genetic crosses were used to recombine the UAS-Snx21-GFP to the prospero-Gal4-containing or tub-Gal4-containing chromosomes.

Immunostaining, tracer uptake assay, and Lysotracker red staining

Tissues from third instar larvae were dissected in PBS and fixed with 4% formaldehyde. Samples were extensively washed with PBS, then incubated in PBTx (0.1% Triton X-100 in PBS) for 30 min. After blocking with 5% FCS-containing PBTx, samples were incubated overnight at 4 °C in the blocking solution completed with primary antibodies. Samples were then rinsed, extensively washed, and then incubated in the blocking solution containing the appropriate secondary antibodies for 2 h at RT. In the case of wing disk samples, blocking was applied prior to incubation with the secondary antibodies as well. After rinsing and washing, nuclei were stained with DAPI. Samples were mounted in Vectashield. The following primary antibodies were used: polyclonal rabbit a-Rab5 (1 : 1000, Abcam #31261), monoclonal mouse a-Rab7 (1 : 10, DSHB), polyclonal chicken a-GFP (1 : 400, Aves Labs #GFP-1020), polyclonal rabbit a-Lamp1 (kindly provided by Andreas Jenny) [66], monoclonal mouse a-Wg (1 : 25, DSHB #4D4), polyclonal rabbit a-HA (1 : 200, Sigma-Aldrich #H6908), monoclonal mouse a-FLAG (DYKDDDDK) tag (1 : 50, Thermo #MA191878). Secondary antibodies were Alexa Fluor 488 goat anti-rabbit, Alexa Fluor 488 goat anti-chicken, Alexa Fluor 568 goat anti-rabbit, Alexa Fluor 568 goat anti-mouse, Alexa Fluor Cy5 goat anti-mouse (all 1 : 800, all Invitrogen–Thermo Fisher). In the case of tracer uptake, nephrocytes of wandering stage larvae were dissected in freshly prepared Shields and Sang M3 insect medium (Sigma-Aldrich #S8398). Cells were incubated in M3 medium completed with BSA Alexa-647 (Thermo Scientific #A34785) at 0,1 mg/mL concentration for 1 or 5 min (pulse), then washed out. Cells containing internalized tracers were then imaged after 10, 15 or 45-min chase interval. For LysoTracker Red staining, nephrocytes were incubated in M3 medium containing LysoTracker Red (1 : 1000; ThermoFisher Scientific # L7528) for 1 min at RT after the chase.

Imaging, quantification and statistical analysis

All stainings have been carried out at least twice (technical replicate), with similar results. Principles of imaging and quantification were the same as described in our previous study [44] and can be shortly summarized as it follows. Images were taken with a Zeiss Axio Imager.M2 fluorescent microscope equipped with ApoTome.2 or a ZEISS LSM 800 confocal microscope with Airyscan using 0.95 NA 40× Plan-Apochromat or 1.4 NA 63× (Oil) Plan-Apochromat objectives, respectively. Images were captured and their brightness and contrast were adjusted uniformly with the Zeiss ZEN Pro software. In general, three to five fields of views, nephrocytes or wing disks per animal were selected for quantification. Images were analyzed with Zeiss ZEN Pro and ImageJ. To measure the size of individual Rab5, Lamp1 or BSA-positive structures, we used the 'Analyze particles' function of ImageJ. Particles under the size 0.02 μm^2 were excluded except for the salivary gland where late endosomes were measured from 0.05 μm^2. To measure the size of individual Rab7-positive structures, we selected the Rab7-positive rings one by one—endosome sizes are profile areas measured in square micron. To quantify BSA-coverage, first we measured the area of individual nephrocytes and the BSA-covered area in each cell, then calculated the BSA-coverage from these values as percentage. For colocalization analyses, we measured Pearson's correlation coefficient of red and green channels (above threshold) using the coloc2 plugin of ImageJ (1 = perfect colocalization, 0 = no/incidental colocalization, and − 1 = mutually exclusive localization). Statistical analysis was performed with GraphPad Prism using the tests indicated in Table S3. A p value of <0.05 is considered to be statistically significant; * means $P < 0.05$; ** means $P < 0.01$; *** means $P < 0.001$, and **** means $P < 0.0001$.

Acknowledgements

We thank Szilvia Bozsó and Erzsébet Fehérné Juhász for technical assistance, Andreas Jenny for providing the a-Lamp1 serum and Vladimir Katanaev for providing the untagged Flo transgenes. This work was supported by the Hungarian Academy of Sciences: Advanced Momentum grant LP2023-6 to GJ, the National Research Development and Innovation Office (NKFIH) of Hungary: PD135611 to TM, K146634 to GJ, and also received support under the 2022-2.1.1-NL funding scheme: 2022-2.1.1-NL-2022-00005. The project received additional funding from the EU's Horizon 2020 research and innovation program: grant agreement 739593, and from the National Academy of Scientist Education under the sponsorship of the Hungarian Ministry of Innovation and Technology: FEIF/646-4/2021-ITM_SZERZ and from the Rollin D. Hotchkiss Foundation.

Author contributions

TM: planned experiments; performed experiments; analyzed data; wrote the paper. EL: performed experiments; analyzed data; wrote the paper. DF: performed

© 2026 The Author(s). *The FEBS Journal* published by John Wiley & Sons Ltd on behalf of Federation of European Biochemical Societies.

17424658, 0, Downloaded from https://febs.onlinelibrary.wiley.com/doi/10.1111/febs.70618 by HUN-REN Biological Research Center, Szeged, Wiley Online Library on [25/11/2026]. See the Terms and Conditions (https://onlinelibrary.wiley.com/terms-and-conditions) on Wiley Online Library for rules of use; OA articles are governed by the applicable Creative Commons License

experiments; analyzed data. GJ: performed experiments. RM: performed experiments. AK: performed experiments; analyzed data. AP: performed experiments; analyzed data. AB: performed experiments; analyzed data. HL: performed experiments; analyzed data. GJ: planned experiments; wrote the paper.

Conflict of interest

The authors declare no conflict of interest.

Peer review

The peer review history for this article is available at https://www.webofscience.com/api/gateway/wos/peer-review/10.1111/febs.70618.

Data availability statement

The data that support the findings of this study are available from the corresponding author [maruzs.tamas@brc.hu] upon reasonable request.

References

1 Huotari J & Helenius A (2011) Endosome maturation. *EMBO J* **30**, 3481–3500. doi: 10.1038/emboj.2011.286

2 Podinovskaia M & Spang A (2018) The endosomal network: mediators and regulators of endosome maturation. *Prog Mol Subcell Biol* **57**, 1–38. doi: 10.1007/978-3-319-96704-2_1

3 kleine Balderhaar HJ & Ungermann C (2013) CORVET and HOPS tethering complexes - coordinators of endosome and lysosome fusion. *J Cell Sci* **126**, 1307–1316. doi: 10.1242/JCS.107805

4 Maxfield FR (2014) Role of endosomes and lysosomes in human disease. *Cold Spring Harb Perspect Biol* **6**, ea016931. doi: 10.1101/cshperspect.a016931

5 Doherty GJ & McMahon HT (2009) Mechanisms of endocytosis. *Annu Rev Biochem* **78**, 857–902. doi: 10.1146/ANNUREV.BIOCHEM.78.081307.110540

6 Bodin S, Elhabashy H, Macdonald E, Winter D & Gauthier-Rouvière C (2025) Flotillins in membrane trafficking and physiopathology. *Biol Cell* **117**, e2400134. doi: 10.1111/BOC.202400134

7 Bickel PE, Scherer PE, Schnitzer JE, Oh P, Lisanti MP & Lodish HF (1997) Flotillin and epidermal surface antigen define a new family of caveolae- associated integral membrane proteins. *J Biol Chem* **272**, 13793–13802. doi: 10.1074/jbc.272.21.13793

8 Volonté D, Galbiati F, Li S, Nishiyama K, Okamoto T & Lisanti MP (1999) Flotillins/Cavatellins are differentially expressed in cells and tissues and form a hetero-oligomeric complex with caveolins *in vivo*. *J Biol Chem* **274**, 12702–12709. doi: 10.1074/jbc.274.18.12702

9 Singh J, Elhabashy H, Muthukottiappan P, Stepath M, Eisenacher M, Kohlbacher O, Gieselmann V & Winter D (2022) Cross-linking of the endolysosomal system reveals potential flotillin structures and cargo. *Nat Commun* **13**, 6212. doi: 10.1038/S41467-022-33951-0

10 Fu Z & MacKinnon R (2024) Structure of the flotillin complex in a native membrane environment. *Proc Natl Acad Sci U S A* **121**, e2409334121. doi: 10.1073/PNAS.2409334121

11 Dermine JF, Duclos S, Garin J, St-Louis F, Rea S, Parton RG & Desjardins M (2001) Flotillin-1-enriched lipid raft domains accumulate on maturing phagosomes. *J Biol Chem* **276**, 18507–18512. doi: 10.1074/jbc.M101113200

12 Langhorst MF, Reuter A & Stuermer CAO (2005) Scaffolding microdomains and beyond: the function of reggie/flotillin proteins. *Cell Mol Life Sci* **62**, 2228–2240. doi: 10.1007/S00018-005-5166-4

13 Planchon D, Rios Morris E, Genest M, Comunale F, Vacher S, Bièche I, Denisov EV, Tashireva LA, Perelmuter VM, Linder S *et al.* (2018) MT1-MMP targeting to endolysosomes is mediated by upregulation of flotillins. *J Cell Sci* **131**, 218925. doi: 10.1242/JCS.218925

14 Stuermer CAO (2010) The reggie/flotillin connection to growth. *Trends Cell Biol* **20**, 6–13. doi: 10.1016/j.tcb.2009.10.003

15 McVeigh BM, de Jesús-Pérez JJ, Siepe DH, Gogoi P, Mageswaran SK, Kalocsay M, Mihelc EM & Moiseenkova-Bell VY (2025) Visualization of lysosomal membrane proteins by cryo electron tomography. *Nat Commun* **16**, 9234. doi: 10.1038/S41467-025-64314-0

16 Affentranger S, Martinelli S, Hahn J, Rossy J & Niggli V (2011) Dynamic reorganization of flotillins in chemokine-stimulated human T-lymphocytes. *BMC Cell Biol* **12**, 28. doi: 10.1186/1471-2121-12-28

17 Langhorst MF, Solis GP, Hannbeck S, Plattner H & Stuermer CAO (2007) Linking membrane microdomains to the cytoskeleton: regulation of the lateral mobility of reggie-1/flotillin-2 by interaction with actin. *FEBS Lett* **581**, 4697–4703. doi: 10.1016/J.FEBSLET.2007.08.074

18 Munderloh C, Solis GP, Bodrikov V, Jaeger FA, Wiechers M, Málaga-Trillo E & Stuermer CAO (2009) Reggies/flotillins regulate retinal axon regeneration in the zebrafish optic nerve and differentiation of hippocampal and N2a neurons. *J Neurosci* **29**, 6607–6615. doi: 10.1523/JNEUROSCI.0870-09.2009

19 Neumann-Glesen C, Fernow I, Amaddii M & Tikkanen R (2007) Role of EGF-induced tyrosine phosphorylation of reggie-1/flotillin-2 in cell spreading and signaling to the actin cytoskeleton. *J Cell Sci* **120**, 395–406. doi: 10.1242/JCS.03336

© 2026 The Author(s). *The FEBS Journal* published by John Wiley & Sons Ltd on behalf of Federation of European Biochemical Societies.

17424658, 0, Downloaded from https://febs.onlinelibrary.wiley.com/doi/10.1111/febs.70618 by HUN-REN Biological Research Center, Szeged, Wiley Online Library on [25/11/2026]. See the Terms and Conditions (https://onlinelibrary.wiley.com/terms-and-conditions) on Wiley Online Library for rules of use; OA articles are governed by the applicable Creative Commons License

20 Rossy J, Schlicht D, Engelhardt B & Niggli V (2009) Flotillins interact with PSGL-1 in neutrophils and, upon stimulation, rapidly organize into membrane domains subsequently accumulating in the uropod. *PLoS One* **4**, e5403. doi: 10.1371/JOURNAL.PONE.0005403
21 Ludwig A, Otto GP, Riento K, Hams E, Fallon PG & Nichols BJ (2010) Flotillin microdomains interact with the cortical cytoskeleton to control uropod formation and neutrophil recruitment. *J Cell Biol* **191**, 771–781. doi: 10.1083/JCB.201005140
22 Bitsikas V, Riento K, Howe JD, Barry NP & Nichols BJ (2014) The role of flotillins in regulating aβ production, investigated using flotillin 1−/−, flotillin 2−/− double knockout mice. *PLoS One* **9**, e85217. doi: 10.1371/JOURNAL.PONE.0085217
23 Gauthier-Rouvière C, Bodin S, Comunale F & Planchon D (2020) Flotillin membrane domains in cancer. *Cancer Metastasis Rev* **39**, 361–374. doi: 10.1007/S10555-020-09873-Y
24 Bodin S, Planchon D, Morris ER, Comunale F & Gauthier-Rouviére C (2014) Flotillins in intercellular adhesion - from cellular physiology to human diseases. *J Cell Sci* **127**, 5139–5147. doi: 10.1242/JCS.159764
25 Zhan Z, Ye M & Xiaofeng JIN (2023) The roles of FLOT1 in human diseases (review). *Mol Med Rep* **28**, 13099. doi: 10.3892/MMR.2023.13099
26 Teasdale RD & Collins BM (2012) Insights into the PX (phox-homology) domain and SNX (sorting nexin) protein families: structures, functions and roles in disease. *Biochem J* **441**, 39–59. doi: 10.1042/BJ20111226
27 Chandra M, Chin YKY, Mas C, Feathers JR, Paul B, Datta S, Chen KE, Jia X, Yang Z, Norwood SJ *et al.* (2019) Classification of the human phox homology (PX) domains based on their phosphoinositide binding specificities. *Nat Commun* **10**, 1528. doi: 10.1038/s41467-019-09355-y
28 Hanley SE & Cooper KF (2020) Sorting nexins in protein homeostasis. *Cells* **10**, 1–26. doi: 10.3390/CELLS10010017
29 Simunovic M, Evergren E, Callan-Jones A & Bassereau P (2019) Curving cells inside and out: roles of BAR domain proteins in membrane shaping and its cellular implications. *Annu Rev Cell Dev Biol* **35**, 111–129. doi: 10.1146/ANNUREV-CELLBIO-100617-060558
30 Clairfeuille T, Norwood SJ, Qi X, Teasdale RD & Collins BM (2015) Structure and membrane binding properties of the endosomal tetratricopeptide repeat (TPR) domain-containing sorting nexins SNX20 and SNX21. *J Biol Chem* **290**, 14504–14517. doi: 10.1074/jbc.M115.650598
31 Danson CM, Pearson N, Heesom KJ & Cullen PJ (2018) Sorting nexin-21 is a scaffold for the endosomal recruitment of huntingtin. *J Cell Sci* **131**, jcs211672.
32 Mostowy S & Cossart P (2012) Septins: the fourth component of the cytoskeleton. *Nat Rev Mol Cell Biol* **13**, 183–194. doi: 10.1038/NRM3284
33 Zeng W, Yuan W, Wang Y, Jiao W, Zhu Y, Huang C, Li D, Li Y, Zhu C, Wu X *et al.* (2002) Expression of a novel member of sorting nexin gene family, SNX-L, in human liver development. *Biochem Biophys Res Commun* **299**, 542–548. doi: 10.1016/S0006-291X(02)02695-5
34 Schaff UY *et al.* (2008) SLIC-1/sorting nexin 20: a novel sorting nexin that directs subcellular distribution of PSGL-1. *Eur J Immunol* **38**, 550–564. doi: 10.1002/EJI.200737777
35 Brant SR, Okou DT, Simpson CL, Cutler DJ, Haritunians T, Bradfield JP, Chopra P, Prince J, Begum F, Kumar A *et al.* (2017) Genome-wide association study identifies African-specific susceptibility loci in African Americans with inflammatory bowel disease. *Gastroenterology* **152**, 206–217. doi: 10.1053/j.gastro.2016.09.032
36 Fan L, Li L, Huang C, Huang S, Deng J & Xiong J (2020) Increased SNX20 and PD-L1 levels can predict the clinical response to PD-1 inhibitors in lung adenocarcinoma. *Onco Targets Ther* **13**, 10075–10085. doi: 10.2147/OTT.S262909
37 Wu GJ, Ren K, He M, Xu JX, Li ZQ, Bo D & Xue Q (2021) SNX20 expression correlates with immune cell infiltration and can predict prognosis in lung adenocarcinoma. *Int J Gen Med* **14**, 7599–7611. doi: 10.2147/IJGM.S337198
38 Chen X, Jiang X, Wang H, Wang C, Wang C, Pan C, Zhou F, Tian J, Niu X, Nie Z *et al.* (2022) DNA methylation-regulated SNX20 overexpression correlates with poor prognosis, immune cell infiltration, and low-grade glioma progression. *Aging* **14**, 5211–5222. doi: 10.18632/AGING.204144
39 Bohdanowicz M & Grinstein S (2013) Role of phospholipids in endocytosis, phagocytosis, and macropinocytosis. *Physiol Rev* **93**, 69–106. doi: 10.1152/PHYSREV.00002.2012
40 Denholm B & Skaer H (2009) Bringing together components of the fly renal system. *Curr Opin Genet Dev* **19**, 526–532. doi: 10.1016/j.gde.2009.08.006
41 Helmstädter M, Huber TB & Hermle T (2017) Using the drosophila nephrocyte to model podocyte function and disease. *Front Media SA* **5**, 262. doi: 10.3389/fped.2017.00262
42 Lund VK, Madsen KL & Kjaerulff O (2018) Drosophila Rab2 controls endosome-lysosome fusion and LAMP delivery to late endosomes. *Autophagy* **14**, 1520–1542. doi: 10.1080/15548627.2018.1458170
43 Lőrincz P, Lakatos Z, Varga Á, Maruzs T, Simon-Vecsei Z, Darula Z, Benkő P, Csordás G, Lippai M, Andó I *et al.* (2016) MiniCORVET is a Vps8-

© 2026 The Author(s). *The FEBS Journal* published by John Wiley & Sons Ltd on behalf of Federation of European Biochemical Societies.

17424658, 0, Downloaded from https://febs.onlinelibrary.wiley.com/doi/10.1111/febs.70618 by HUN-REN Biological Research Center, Szeged, Wiley Online Library on [25/11/2026]. See the Terms and Conditions (https://onlinelibrary.wiley.com/terms-and-conditions) on Wiley Online Library for rules of use; OA articles are governed by the applicable Creative Commons License

containing early endosomal tether in drosophila. *Elife* **5**, e14226. doi: 10.7554/ELIFE.14226
44 Maruzs T, Feil-Börcsök D, Lakatos E, Juhász G, Blastyák A, Hargitai D, Jean S, Lőrincz P & Juhász G (2023) Interaction of the sorting nexin 25 homologue Snazarus with Rab11 balances endocytic and secretory transport and maintains the ultrafiltration diaphragm in nephrocytes. *Mol Biol Cell* **34**, ar87. doi: 10.1091/mbc.E22-09-0421
45 Kim S, Wairkar YP, Daniels RW & DiAntonio A (2010) The novel endosomal membrane protein ema interacts with the class C Vps-HOPS complex to promote endosomal maturation. *J Cell Biol* **188**, 717–734. doi: 10.1083/jcb.200911126
46 Vanlandingham PA & Ceresa BP (2009) Rab7 regulates late endocytic trafficking downstream of multivesicular body biogenesis and cargo sequestration. *J Biol Chem* **284**, 12110–12124. doi: 10.1074/JBC.M809277200
47 Bucci C, Thomsen P, Nicoziani P, McCarthy J & van Deurs B (2000) Rab7: a key to lysosome biogenesis. *Mol Biol Cell* **11**, 467–480.
48 Boda A, Balázs V, Nagy A, Hargitai D, Lippai M, Simon-Vecsei Z, Molnár M, Fürstenhoffer F, Juhász G & Lőrincz P (2025) The Rab7-Epg5 and Rab39-ema modules cooperatively position autophagosomes for efficient lysosomal fusions. *Elife* **13**, e102663. doi: 10.7554/ELIFE.102663
49 Hegedus K *et al.* (2016) The Ccz1-Mon1-Rab7 module and Rab5 control distinct steps of autophagy. *Mol Biol Cell* **27**, 3132–3142. doi: 10.1091/MBC.E16-03-0205
50 Bucci C, Parton RG, Mather IH, Stunnenberg H, Simons K, Hoflack B & Zerial M (1992) The small GTPase rab5 functions as a regulatory factor in the early endocytic pathway. *Cell* **70**, 715–728. doi: 10.1016/0092-8674(92)90306-W
51 Atienza-Manuel A, Castillo-Mancho V, de Renzis S, Culi J & Ruiz-Gómez M (2021) Endocytosis mediated by an atypical CUBAM complex modulates slit diaphragm dynamics in nephrocytes. *Development* **148**, e199894. doi: 10.1242/dev.199894
52 Vázquez CL & Colombo MI (2009) Chapter 6 assays to assess autophagy induction and fusion of autophagic vacuoles with a degradative compartment, using Monodansylcadaverine (MDC) and DQ-BSA. *Methods Enzymol* **451**, 85–95. doi: 10.1016/S0076-6879(08)03606-9
53 Lang K, Milosavljevic J, Heinkele H, Chen M, Gerstner L, Spitz D, Kayser S, Helmstädter M, Walz G, Köttgen M *et al.* (2022) Selective endocytosis controls slit diaphragm maintenance and dynamics in drosophila nephrocytes. *Elife* **11**, e79037. doi: 10.7554/ELIFE.79037
54 Hoehne M, De Couet HG, Stuermer CAO & Fischbach KF (2005) Loss- and gain-of-function analysis of the lipid raft proteins Reggie/flotillin in drosophila: they are posttranslationally regulated, and misexpression interferes with wing and eye development. *Mol Cell Neurosci* **30**, 326–338. doi: 10.1016/j.mcn.2005.07.007
55 Katanaev VL, Solis GP, Hausmann G, Buestorf S, Katanayeva N, Schrock Y, Stuermer CAO & Basler K (2008) Reggie-1/flotillin-2 promotes secretion of the long-range signalling forms of wingless and hedgehog in drosophila. *EMBO J* **27**, 509–521. doi: 10.1038/SJ.EMBOJ.7601981
56 Glebov OO, Bright NA & Nichols BJ (2006) Flotillin-1 defines a clathrin-independent endocytic pathway in mammalian cells. *Nat Cell Biol* **8**, 46–54. doi: 10.1038/NCB1342
57 Frick M, Bright NA, Riento K, Bray A, Merrified C & Nichols BJ (2007) Coassembly of Flotillins induces formation of membrane microdomains, membrane curvature, and vesicle budding. *Curr Biol* **17**, 1151–1156. doi: 10.1016/j.cub.2007.05.078
58 Solis GP, Hülsbusch N, Radon Y, Katanaev VL, Plattner H & Stuermer CAO (2013) Reggies/flotillins interact with Rab11a and SNX4 at the tubulovesicular recycling compartment and function in transferrin receptor and E-cadherin trafficking. *Mol Biol Cell* **24**, 2689–2702. doi: 10.1091/MBC.E12-12-0854
59 Tanaka-Takiguchi Y, Kinoshita M & Takiguchi K (2009) Septin-mediated uniform bracing of phospholipid membranes. *Curr Biol* **19**, 140–145. doi: 10.1016/j.cub.2008.12.030
60 Bridges AA, Zhang H, Mehta SB, Occhipinti P, Tani T & Gladfelter AS (2014) Septin assemblies form by diffusion-driven annealing on membranes. *Proc Natl Acad Sci U S A* **111**, 2146–2151. doi: 10.1073/PNAS.1314138111
61 Traikov S, Stange C, Wassmer T, Paul-Gilloteaux P, Salamero J, Raposo G & Hoflack B (2014) Septin6 and Septin7 GTP binding proteins regulate AP-3- and ESCRT-dependent multivesicular body biogenesis. *PLoS One* **9**, e109372. doi: 10.1371/JOURNAL.PONE.0109372
62 Dolat L & Spiliotis ET (2016) Septins promote macropinosome maturation and traffic to the lysosome by facilitating membrane fusion. *J Cell Biol* **214**, 517–527. doi: 10.1083/JCB.201603030
63 Laczkó-Dobos H, Bhattacharjee A, Maddali AK, Kincses A, Abuammar H, Sebők-Nagy K, Páli T, Dér A, Hegedűs T, Csordás G *et al.* (2024) PtdIns4P is required for the autophagosomal recruitment of STX17 (syntaxin 17) to promote lysosomal fusion. *Autophagy* **20**, 1639–1650. doi: 10.1080/15548627.2024.2322493
64 Laczkó-Dobos H, Maddali AK, Jipa A, Bhattacharjee A, Végh AG & Juhász G (2021) Lipid profiles of autophagic structures isolated from wild type and Atg2

© 2026 The Author(s). *The FEBS Journal* published by John Wiley & Sons Ltd on behalf of Federation of European Biochemical Societies.

17424658, 0, Downloaded from https://febs.onlinelibrary.wiley.com/doi/10.1111/febs.70618 by HUN-REN Biological Research Center, Szeged, Wiley Online Library on [25/11/2026]. See the Terms and Conditions (https://onlinelibrary.wiley.com/terms-and-conditions) on Wiley Online Library for rules of use; OA articles are governed by the applicable Creative Commons License

mutant drosophila. *Biochim Biophys Acta* **1866**, 158868. doi: 10.1016/j.bbalip.2020.158868

65 Bechtel W, Helmstädter M, Balica J, Hartleben B, Kiefer B, Hrnjic F, Schell C, Kretz O, Liu S, Geist F *et al*. (2013) Vps34 deficiency reveals the importance of endocytosis for podocyte homeostasis. *J Am Soc Nephrol* **24**, 727–743. doi: 10.1681/ASN.2012070700/-/DCSUPPLEMENTAL

66 Chaudhry N, Sica M, Surabhi S, Hernandez DS, Mesquita A, Selimovic A, Riaz A, Lescat L, Bai H, GC MI *et al*. (2022) Lamp1 mediates lipid transport, but is dispensable for autophagy in drosophila. *Autophagy* **18**, 2443–2458. doi: 10.1080/15548627.2022.2038999

Supporting information

Additional supporting information may be found online in the Supporting Information section at the end of the article.

Fig. S1. Full-length Drosophila Snx21 tagged with GFP on its N or C terminus displays similar distribution pattern across larval fly tissues.

Fig. S2. Overexpression of untagged flotillins causes ectopic wing vein formation.

Table S1. Details of statistical tests used in the study.

© 2026 The Author(s). *The FEBS Journal* published by John Wiley & Sons Ltd on behalf of Federation of European Biochemical Societies.

17424658, 0, Downloaded from https://febs.onlinelibrary.wiley.com/doi/10.1111/febs.70618 by HUN-REN Biological Research Center, Szeged, Wiley Online Library on [25/11/2026]. See the Terms and Conditions (https://onlinelibrary.wiley.com/terms-and-conditions) on Wiley Online Library for rules of use; OA articles are governed by the applicable Creative Commons License